Efficient Design of Oversampled NPR GDFT Filterbanks

Matthew R. Wilbur, *Member, IEEE*, Timothy N. Davidson, *Member, IEEE*, and James P. Reilly, *Member, IEEE*

***Abstract*—We propose a flexible, efficient design technique for the prototype filter of an oversampled near perfect reconstruction (NPR) generalized discrete Fourier transform (GDFT) filterbank. Such filterbanks have several desirable properties for subband processing systems that are sensitive to aliasing, such as subband adaptive filters. The design criteria for the prototype filter are explicit bounds (derived herein) on the aliased components in the subbands and the output, the distortion induced by the filterbank, and the imaged subband errors in the output. It is shown that the design of an optimal prototype filter can be transformed into a convex optimization problem, which can be efficiently solved. The proposed design technique provides an efficient and effective tool for exploring many of the inherent tradeoffs in the design of the prototype filter, including the tradeoff between aliasing in the subbands and the distortion induced by the filterbank. We calculate several examples of these tradeoffs and demonstrate that the proposed method can generate filters with significantly better performance than filters obtained using current design methods.**

***Index Terms*—Adaptive filters, convex optimization, modulated filterbanks, oversampled filterbanks, subband filtering.**

I. Introduction

UNIFORM multirate filterbanks form the basic unit of many multirate signal processing systems in a diverse set of applications that includes audio and image compression, denoising, feature detection and extraction, and adaptive filtering [1]–[4]. A typical example of such a system is illustrated in Fig. 1. The standard design techniques for uniform filterbanks are based on (approximating) the perfect reconstruction condition that in the absence of any subband processing, the output signal is simply a scaled and delayed version of the input [1]–[4]. It is now well known that perfect reconstruction can be (exactly) achieved with finite impulse response (FIR) filters in both the critically sampled $(K = M)$ and oversampled $(K < M)$ arrangements [2]–[6]. Classes of efficiently implementable "modulated" filterbanks are also available [1]–[4], [7]–[10]. However, it is becoming apparent that perfect reconstruction filterbanks do not necessarily provide optimal performance of the subband signal processing system as a whole, e.g., [11]. Designs based on the perfect reconstruction condition typically allow considerable aliasing in the subband signals $s_m[k]$ but structure these aliased components so that in the absence of any subband processing, they are cancelled by the synthesis filterbank. This characteristic may be undesirable if the subband processing block is sensitive to aliasing in the subband signals or if the subband processing block distorts the aliased components in the subband signals in a way that reduces the effectiveness of alias cancellation. An application that is particularly sensitive to aliasing in the subbands is subband adaptive filtering [12]–[17]. The subband processing block of a subband adaptive filtering system typically consists of a diagonal matrix of adaptive filters, each of which operates on one of the subband signals, and operates independently of the other adaptive filters.[1] The objective of the subband processing block is, quite naturally, to filter the subband signals. However, by doing so, it may distort the aliased components in the subband signals and, hence, reduce the effectiveness of alias cancellation.

For subband adaptive filtering, and other applications with similar characteristics, near-perfect reconstruction (oversampled) filterbanks that *suppress* aliasing in the subbands and "imaging" [2] of the subband errors in the output, rather than relying on *cancellation*, offer the potential for improved performance. In particular, the performance of systems based on the class of oversampled generalized discrete Fourier transform (GDFT) filterbanks is quite encouraging [16]–[22]. These filterbanks are better able to suppress aliasing in the subbands than (uniform) oversampled cosine-modulated filterbanks [18], [19], [21] and can be efficiently implemented using the GDFT [1]. In this paper, we propose a flexible, efficient design technique for the prototype filter of an oversampled near perfect reconstruction (NPR) GDFT filterbank. The design criteria are explicit bounds (derived herein) on the aliased components in the subbands (and the output), the imaged subband error components in the output, and the distortion induced by the filterbank. These bounds rigorously amalgamate several intuitively developed design criteria in the current literature [15], [18]–[22] and subsume the criteria derived in [16, Section IV-B] and [23]. The proposed design criteria generate familiar constraints on the prototype filter: The aliasing criteria result in bounds on the stopband energy and the maximum stopband level, the imaging criterion results in an additional bound on the transition-band energy, and the distortion criterion results in a measure of the distance between the prototype filter and a "self-orthogonal" filter.

Manuscript received August 19, 2002; revised August 11, 2003. The associate editor coordinating the review of this manuscript and approving it for publication was Dr. Henrique Malvar.

The authors are with the Department of Electrical and Computer Engineering, McMaster University, Hamilton, ON, L8S 4K1, Canada (e-mail: davidson@mcmaster.ca; reillyj@mcmaster.ca).

Digital Object Identifier 10.1109/TSP.2004.828936

[1]The use of off-diagonal "cross" filters [13] can reduce the sensitivity to aliasing but may adversely affect the convergence properties of the adaptive filter and increases the computational cost of the system.

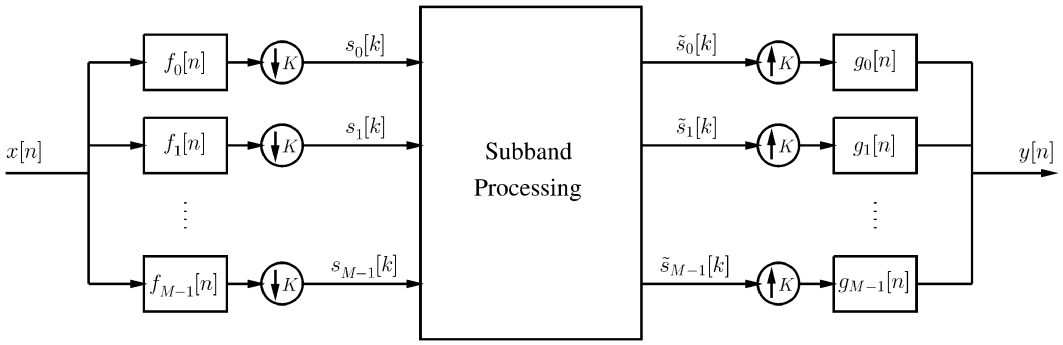

Fig. 1. M-channel uniform subband signal processing system.

In their direct form, these constraints generate a nonconvex feasible set. Therefore, careful detection and management of locally optimal solutions may be required in order to obtain a filter that achieves an objective value sufficiently close to that of a globally optimal prototype.[2] The key step in obtaining the proposed efficient design technique is to show that the design criteria can be (precisely) transformed into convex functions of the (deterministic) autocorrelation of the prototype filter and, hence, that a (globally) optimal prototype filter can be obtained from the solution of a convex optimization problem that can be efficiently solved. A feature of the proposed method is that the semi-infinite constraints generated by the maximum stopband level constraint and the constraint that the autocorrelation can be spectrally factorized are transformed into (finite) linear matrix inequalities.

The convex formulation of the design problem not only provides an efficient algorithm for finding an optimal prototype filter, but by doing so, it provides an efficient method for determining the inherent tradeoffs between competing prototype design criteria. Of particular interest is the inherent tradeoff between aliasing in the subbands and the distortion induced by the filterbank. We calculate several examples of these tradeoffs and demonstrate that filters designed via the proposed formulation can provide significantly better performance than filters designed using current methods.

The paper is arranged as follows: In Section II, we describe the class of GDFT filterbanks and discuss the relationships between the proposed design method and current techniques in greater detail. In Section III, we derive the design criteria, and in Section IV, we provide the transformation to the convex design problem. In Section V, we demonstrate how the proposed method generates filters that achieve certain inherent design tradeoffs, and in Section VI, we illustrate how this leads to improved performance over filters designed by two competing methods.

II. GDFT Filterbanks

The generalized discrete Fourier transform (GDFT) filterbank [1] we will consider is of the form in Fig. 1, with the analysis and synthesis filters consisting of exponentially modulated versions of a single real-valued FIR prototype filter $p[n]$:

$$f_m[n] = p[n]e^{j2\pi(m+m_0)(n+n_0)/M} \tag{1a}$$

$$g_m[n] = f_m[-n]^* = p[-n]e^{j2\pi(m+m_0)(n-n_0)/M} \tag{1b}$$

where m_0 and n_0 are frequency-shift and phase-shift constants, respectively. Such filterbanks can be efficiently implemented using the GDFT [1]. It is well known that the only critically sampled filterbanks of the form in (1) with perfect reconstruction (PR) are those generated by a prototype filter that is a length-M rectangular window [25]. Such a prototype filter leads to substantial aliasing in the subbands. Moreover, critically sampled near perfect reconstruction (NPR) filterbanks of the form in (1) have approximately the same prototype. In the oversampled case, there are longer prototypes that generate PR and NPR filterbanks of the form in (1), and hence, prototypes that generate much lower aliasing in the subbands can be obtained. The focus of this paper is on NPR filterbanks because the effectiveness of the alias cancellation in PR filterbanks may be compromised by the subband processing and because improved alias suppression in the subbands and image suppression in the output can be achieved by relaxing the PR constraint. The fact that we employ the same prototype filter in the analysis and synthesis banks means that our NPR filterbanks have polyphase matrices [2], which are nearly paraunitary, and hence have favorable noise robustness and numerical properties.

One possible approach to the design of oversampled GDFT filterbanks is to use the fact that any prototype filter for an L-times oversampled PR cosine-modulated filterbank is a prototype for a $2L$-times oversampled PR DFT filterbank [9], [10]. The design of prototype filters for NPR and PR cosine-modulated filterbanks is usually expressed as a constrained optimization problem for the filter coefficients [26], [27] or as an unconstrained optimization problem over some alternative variables (in some cases called lattice coefficients), which are related to the filter coefficients in such a way that PR is automatically satisfied [29]. Unfortunately, the constraints in the former method and the objective in the latter are nonconvex functions of the design parameters, and hence, these formulations can be quite awkward to solve. Furthermore, exploiting the relationship with cosine-modulated filterbanks generates a

[2]Rigorous methods (e.g., [24]) are effective but tend to be computationally expensive. Simpler techniques, such as running a standard local optimization algorithm from multiple starting points, are less expensive but may not be as effective.

subclass of the (G)DFT filterbanks but not the whole class [9], [10]. As one might expect, direct formulation of the design of a GDFT prototype (over the whole available class) also leads to nonconvex optimization problems [16], [18], [19], [22]. (Some simple, but *ad hoc*, prototype design methods have also been proposed [15], [20].) The approach we outline in this paper involves the transformation[3] of the design into a convex optimization problem in which the autocorrelation coefficients of the prototype are the design variables. This convex optimization problem can be efficiently solved for the (globally) optimal autocorrelation, from which an optimal prototype can be obtained via spectral factorization. A number of methods of spectral factorization are described in [30] and [35]. The simplicity of autocorrelation-based prototype design has been recognized before [36], in the context of cosine-modulated filterbanks. However, in [36], the transformation of the design criteria into functions of the autocorrelation sequence involves approximations, and these approximations manifest themselves in undesirable properties of the prototype. In contrast, our design transformation is precise, and since our design criteria are explicit bounds on the aliasing, imaging and distortion energies, we obtain prototype filters with many desirable properties.

III. Derivation of Design Criteria

In this section, we establish design criteria for the prototype filter that enable us to control the aliased components that appear in the subband signals $s_m[k]$, the imaged components that appear in the output, and the distortion induced by the filterbank. As discussed in the Introduction and studied in greater detail in [16] and [17], the performance of a GDFT-filterbank-based subband adaptive filter is critically dependent on these terms.

If $X(z) = \sum_n x[n]z^{-n}$ denotes the z-transform of the input signal, then the mth subband signal in Fig. 1 has a z-transform

$$S_m(z) = \frac{1}{K}F_m(z^{1/K})X(z^{1/K}) + \frac{1}{K}\sum_{k=1}^{K-1} F_m(z^{1/K}W_K^k)X(z^{1/K}W_K^k) \quad (2)$$

where $W_K = e^{-j2\pi/K}$. The first term on the right-hand side of (2) represents the desired component of the subband signal, and the second term represents the aliased components.

The nature of the output of the subband processing system in Fig. 1 clearly depends on the nature of the subband processing block. In subband adaptive filtering applications, the subband processing block typically consists of a diagonal matrix of adaptive filters. If the adaptive filter in the mth subband has converged to $H_m(z)$ [and is "frozen" from that point], then the subband outputs are $\tilde{S}_m(z) = H_m(z)S_m(s)$, and the output of the system in Fig. 1 is

$$\begin{aligned} Y(z) &= \sum_{m=0}^{M-1} G_m(z)\tilde{S}_m(s) \\ &= \frac{1}{K}\sum_{m=0}^{M-1} G_m(z)H_m(z^K)F_m(z)X(z) \\ &\quad + \frac{1}{K}\sum_{m=0}^{M-1} G_m(z)H_m(z^K) \\ &\quad \times \sum_{k=1}^{K-1} F_m(zW_K^k)X(zW_K^k). \end{aligned} \quad (3)$$

If there is no subband processing, then $H_m(z) = 1$, and (3) simplifies to the standard expression for the output of a filterbank [1]–[4]. The transfer function $D(z) = (1/K)\sum_{m=0}^{M-1} G_m(z)H_m(z^K)F_m(z)$ in (3) describes the processing of the input signal $X(z)$, whereas the second term in (3) represents the aliased components that appear at the output. In Sections III-A–D, we will analyze the aliased components in (2) and (3), the undesired distortion induced by the filterbank, and the imaged components of errors in $\tilde{S}_m(z)$ that appear in the output. We will show how the energy of each term can be bounded by natural properties of the prototype filter. For simplicity, our analysis is based on a deterministic input signal $x[n]$, but a complementary analysis based on a stochastic model for $x[n]$ can also be performed.

A. Aliasing in the Subbands

Our analysis of the aliased components in the mth subband signal $s_m[k]$ will be expedited by considering an upsampled version of $s_m[k]$, which has the same sample rate as $x[n]$. This signal will be denoted by $v_m[n]$, where $v_m[kK] = s_m[k]$, and $v_m[kK+i] = 0$, $i = 1, 2, \ldots, K-1$. Since upsampling does not change the energy of the signal, and since the spectrum of $v_m[n]$ is periodic (in frequency) with period $2\pi/K$, the energy of $s_m[k]$ can be computed from $v_m[n]$ as follows:

$$E_{s_m} = \frac{1}{2\pi}\int_{-\pi}^{\pi} \left|S_m(e^{j\omega})\right|^2 d\omega = \frac{1}{2\pi}\int_{\Omega} \left|V_m(e^{j\omega})\right|^2 d\omega \quad (4)$$

where Ω is an interval of width $2\pi/K$. For our analysis, a convenient interval is

$$\Omega_M^m = \left\{\omega : \frac{2\pi(m+m_0)}{M} - \frac{\pi}{K} \le \omega < \frac{2\pi(m+m_0)}{M} + \frac{\pi}{K}\right\} \quad (5)$$

which is the principal spectral support of the mth analysis filter in a GDFT filterbank. To simplify some of our expressions, we define

$$\alpha_m = \frac{2\pi(m+m_0)}{M} \text{ and } \psi_k = \frac{2\pi k}{K}. \quad (6)$$

[3]Similar transformations have also led to convex formulations of some other FIR filter design problems [30]–[34], but the design problems considered herein are specially tailored to the design of prototype filters for oversampled NPR GDFT filterbanks.

Using (4) and (2), the energy of the aliased components in the mth subband signal for a deterministic signal $x[n]$ is

$$E_{A_m} = \frac{1}{2\pi} \times \int_{\omega\in\Omega_M^m} \left| \frac{1}{K} \sum_{k=1}^{K-1} F_m\left(e^{j(\omega-\psi_k)}\right) X\left(e^{j(\omega-\psi_k)}\right) \right|^2 d\omega. \quad (7)$$

Setting $\phi = \omega - \alpha_m$ and using the fact (1) that $F_m(e^{j\omega}) = e^{j\alpha_m n_0} P(e^{j(\omega-\alpha_m)})$, where $P(e^{j\omega})$ is the frequency response of the prototype filter, we have that

$$\begin{aligned} E_{A_m} &= \frac{1}{2\pi} \int_{-\pi/K}^{\pi/K} \left| \frac{1}{K} \sum_{k=1}^{K-1} P\left(e^{j(\phi-\psi_k)}\right) \times X\left(e^{j(\phi+\alpha_m-\psi_k)}\right) \right|^2 d\phi \\ &= \frac{1}{2\pi K^2} \sum_{k,\ell=1}^{K-1} \int_{-\pi/K}^{\pi/K} P(e^{j(\phi-\psi_k)}) P^*\left(e^{j(\phi-\psi_\ell)}\right) \times X\left(e^{j(\phi+\alpha_m-\psi_k)}\right) X^*\left(e^{j(\phi+\alpha_m-\psi_\ell)}\right) d\phi. \quad (8) \end{aligned}$$

We will now develop bounds for E_{A_m} under the assumption that $\sum_n |x[n]|$ is finite. This assumption ensures that the signal energy $E_x = \sum_n |x[n]|^2$ and

$$U_X \triangleq \max_\omega \left|X(e^{j\omega})\right| \quad (9)$$

are finite. The assumption also ensures that

$$J_X(\mu) \triangleq \frac{1}{2\pi} \int_{-\pi}^{\pi} \left|X(e^{j\omega}) X^*(e^{j(\omega+\mu)})\right| d\omega \quad (10)$$

is finite for all μ. (The term $J_X(\mu)$ is closely related to the spectral correlation [37] of $x[n]$ for a frequency separation of μ.) Note that $J_X(0) = E_x$ and that $J_X(-\mu) = J_X(\mu)$. Since $J_X(\mu)$ is finite, the following portion of $J_X(\mu)$ is also finite:

$$\tilde{J}_X(\mu_1,\mu_2,\alpha) \triangleq \frac{1}{2\pi} \int_{-\pi/K+\alpha}^{\pi/K+\alpha} \left|X(e^{j(\omega-\mu_1)}) X^*(e^{j(\omega-\mu_2)})\right| d\omega. \quad (11)$$

By taking the absolute value of the integrand in (8) and extracting the terms dependent on the prototype filter, we obtain the following bound on E_{A_m}:

$$\begin{aligned} E_{A_m} &\le \frac{1}{2\pi K^2} \times \sum_{k,\ell=1}^{K-1} \max_{\phi\in[-\pi/K,\pi/K]} \left|P(e^{j(\phi-\psi_k)}) P^*(e^{j(\phi-\psi_\ell)})\right| \times \int_{-\pi/K+\alpha_m}^{\pi/K+\alpha_m} \left|X(e^{j(\lambda-\psi_k)}) X^*(e^{j(\lambda-\psi_\ell)})\right| d\lambda \quad (12) \\ &= \frac{1}{K^2} \sum_{k,\ell=1}^{K-1} \max_{\phi\in[-\pi/K,\pi/K]} \left|P(e^{j(\phi-\psi_k)}) P^*(e^{j(\phi-\psi_\ell)})\right| \times \tilde{J}_X(\psi_k,\psi_\ell,\alpha_m). \quad (13) \end{aligned}$$

Let $U_P \triangleq \max_\omega |P(e^{j\omega})|$ denote the maximal spectral component of the prototype, and let $U_{P,\mathrm{sb}} \triangleq \max_{\omega\in[\pi/K,2\pi-\pi/K]} |P(e^{j\omega})|$, with $U_{P,\mathrm{sb}} \le U_P$, denote the maximum sidelobe level of the prototype. That is, let the prototype filter satisfy a spectral mask of the form shown in Fig. 2. Since $k,\ell \ge 1$, we have that

$$\begin{aligned} &\max_{\phi\in[-\pi/K,\pi/K]} \left|P(e^{j(\phi-\psi_k)}) P^*(e^{j(\phi-\psi_\ell)})\right| \\ &\quad \le \max_{\phi\in[-\pi/K,\pi/K]} \left|P(e^{j(\phi-\psi_k)})\right| \times \max_{\phi\in[-\pi/K,\pi/K]} \left|P^*(e^{j(\phi-\psi_\ell)})\right| \\ &\quad = U_{P,\mathrm{sb}}^2. \end{aligned} \quad (14)$$

Hence

$$E_{A_m} \le \frac{U_{P,\mathrm{sb}}^2}{K^2} \sum_{k,\ell=1}^{K-1} \tilde{J}_X(\psi_k,\psi_\ell,\alpha_m). \quad (15)$$

Equation (15) is an explicit bound for the energy of the aliased components in each subband signal and is a simple multiple of the square of the maximum stopband level of the prototype filter.

An alternative bound on E_{A_m} can be obtained by writing $E_{A_m} = E_{A_{m,a}} + E_{A_{m,b}}$, where $E_{A_{m,a}}$ contains the terms in (8) with $\ell = k$, and $E_{A_{m,b}}$ contains the remaining terms. Using the technique used to obtain (15), $E_{A_{m,b}}$ can be bounded as $E_{A_{m,b}} \le \left(U_{P,\mathrm{sb}}^2/K^2\right) \sum_{k=1}^{K-1} \sum_{\ell=1,\ell\ne k}^{K-1} \tilde{J}_X(\psi_k,\psi_\ell,\alpha_m)$. The remaining term is

$$\begin{aligned} E_{A_{m,a}} &= \frac{1}{2\pi K^2} \sum_{k=1}^{K-1} \int_{-\pi/K}^{\pi/K} \left|P(e^{j(\phi-\psi_k)}) X(e^{j(\phi+\alpha_m-\psi_k)})\right|^2 d\phi \\ &= \frac{1}{2\pi K^2} \int_{-2\pi+\pi/K}^{-\pi/K} \left|P(e^{j\phi})\right|^2 \left|X(e^{j(\phi+\alpha_m)})\right|^2 d\phi \\ &\le E_{P,\mathrm{sb}} \frac{U_X^2}{K^2} \end{aligned} \quad (16)$$

where the last step is obtained by applying the Hölder inequality [38] and observing that

$$\max_{\theta\in[-2\pi+\pi/K,-\pi/K]} \left|X(e^{j(\theta+\alpha_m)})\right| \le U_X.$$

The term $E_{P,\mathrm{sb}}$ is the stopband energy of the filter

$$E_{P,\mathrm{sb}} = \frac{1}{2\pi} \int_{\pi/K}^{2\pi-\pi/K} \left|P(e^{j\theta})\right|^2 d\theta. \quad (17)$$

Hence, we have the following alternative bound to that in (15)

$$E_{A_m} \le E_{P,\mathrm{sb}} \frac{U_X^2}{K^2} + \frac{U_{P,\mathrm{sb}}^2}{K^2} \sum_{k=1}^{K-1} \sum_{\substack{\ell=1 \\ \ell\ne k}}^{K-1} \tilde{J}_X(\psi_k,\psi_\ell,\alpha_m) \quad (18)$$

which is a linear combination of the stopband energy and the square of the maximum stopband level of the prototype filter.

B. Aliasing in the Output

The analysis of the aliased components in the output of the subband processing system is more difficult than that of the aliased components in the subbands because it depends on the nature of the subband processing. However, for the adaptive filtering scenario described at the beginning of Section III, we can determine the energy of the aliased components in the output by

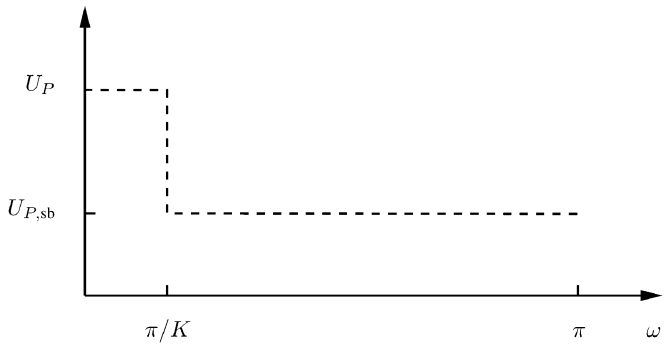

Fig. 2. Mask on the magnitude spectrum of the prototype filter.

evaluating the energy of the second term on the right-hand side of (3). That is

$$E_{A_{\mathrm{out}}} = \frac{1}{2\pi}\int_{-\pi}^{\pi}\left|\frac{1}{K}\sum_{m=0}^{M-1}\sum_{k=1}^{K-1} G_m(e^{j\omega})H_m(e^{jK\omega}) \times F_m(e^{j(\omega-\psi_k)})X(e^{j(\omega-\psi_k)})\right|^2 d\omega. \quad (19)$$

Using techniques akin to those used to derive (18) (the details of which have been omitted for brevity), we can obtain the following bound for $E_{A_{\mathrm{out}}}$:

$$E_{A_{\mathrm{out}}} \le \frac{U_P^2}{K^2}\left(E_{P,\mathrm{sb}}KU_X^2\left(\sum_m U_{H_m}^2\right) + U_{P,\mathrm{sb}}^2\sum_{k=1}^{K-1}\sum_{\substack{\ell=1\\ \ell\neq k}}^{K-1}\sum_{m=0}^{M-1}\sum_{\substack{n=0\\ n\neq m}}^{M-1}\Gamma_X(m,n,k,\ell)\right) \quad (20)$$

where $U_{H_m} \triangleq \max_\omega |H_m(e^{j\omega})|$, and

$$\Gamma_X(m,n,k,\ell) = \frac{1}{2\pi}\int_{-\pi}^{\pi}\Big|H_m(e^{jK\omega})H_n^*(e^{jK\omega}) \times X(e^{j(\omega-\psi_k)})X^*(e^{j(\omega-\psi_\ell)})\Big|d\omega. \quad (21)$$

This bound consists of simple functions of the maximum stopband level, the stopband energy, and the maximum component of the spectrum of the prototype filter. If the adaptive filters are such that $U_{H_m} \le 1$, then $\Gamma_X(m,n,k,\ell) \le J_X(\psi_{k-\ell})$, where $J_X(\mu)$ was defined in (10), and we can obtain the following simplified bound:

$$E_{A_{\mathrm{out}}} \le U_P^2\frac{M}{K^2}\left(E_{P,\mathrm{sb}}KU_X^2 + U_{P,\mathrm{sb}}^2(M-1)\sum_{k=1}^{K-1}\sum_{\substack{\ell=1\\ \ell\neq k}}^{K-1} J_X(\psi_{k-\ell})\right). \quad (22)$$

C. Distortion in the Output

The third performance measure for the filterbank is the distortion that it induces on the signal. In order to isolate the (undesirable) distortion induced by the filterbank from the (desired) processing performed by the subband processing block, we will analyze the distortion in the absence of any subband processing, that is, with $H_m(z) = 1$ in (3). If the filterbank is distortion-free, then $(1/K)\sum_{m=0}^{M-1} G_m(z)F_m(z) = cz^{-d}$, where c is a constant, and d is an integer [2]–[4]. In that case, the first term in (3) becomes

$$\frac{1}{K}\sum_{m=0}^{M-1} G_m(z)F_m(z)X(z) = cX(z)z^{-d}.$$

Without loss of generality in the design criteria for the prototype filter, we can restrict our attention to the case where the output is neither scaled nor delayed, i.e., where $c = 1$ and $d = 0$. In that case, the energy of the distortion induced by the filterbank is

$$\begin{aligned} E_D &= \frac{1}{2\pi}\int_{-\pi}^{\pi}\left|\frac{1}{K}\sum_{m=0}^{M-1} G_m(e^{j\omega})F_m(e^{j\omega})X(e^{j\omega}) - X(e^{j\omega})\right|^2 d\omega \\ &= \frac{1}{2\pi}\int_{-\pi}^{\pi}\left|\left(\frac{1}{K}\sum_{m=0}^{M-1}\left|P(e^{j(\omega-\alpha_m)})\right|^2 - 1\right) \times X(e^{j\omega})\right|^2 d\omega. \end{aligned} \quad (23)$$

This may be bounded in the following way:

$$E_D \le \frac{U_X^2}{2\pi}\int_{-\pi}^{\pi}\left|\frac{1}{K}\sum_{m=0}^{M-1}\left|P(e^{j(\omega-\alpha_m)})\right|^2 - 1\right| d\omega \quad (24)$$

$$= U_X^2\sum_n\left|\sum_\ell \frac{M}{K}p[\ell]p[\ell-nM] - \delta[n]\right|^2 \quad (25)$$

where $\delta[n]$ is the Kronecker delta, and we have used Parseval's relation. [The derivation of (25) is analogous to that of (43) in the Appendix, for which more details are provided.] If we normalize the energy of the prototype filter so that $\sum_\ell p[\ell]^2 = K/M$, then

$$E_D \le \gamma_p^2\frac{MU_X^2}{K} \quad (26)$$

where

$$\gamma_p^2 = \sum_{\substack{n\\ n\neq 0}}\left|\sum_\ell p[\ell]p[\ell-nM]\right|^2. \quad (27)$$

As shown in the Appendix, for a normalized prototype, the energy of the distortion in the output can also be bounded by

$$E_D \le \tilde{\gamma}_p^2\frac{ME_x}{K} \quad (28)$$

where $\tilde{\gamma}_p = \sum_{n,n\neq 0}\sum_\ell |p[\ell]p[\ell-nM]|$ and, as previously defined, $E_x = \sum_n x[n]^2$ is the energy of the input signal. In this paper, we will focus on the bound on E_D in (26), but previous work in a different application [34] suggests that using the bound in (28) will generate qualitatively similar results. This is because both γ_p and $\tilde{\gamma}_p$ are measures of the "distance" between $p[\ell]$ and a filter $q[\ell]$, which satisfies $\sum_\ell q[\ell]q[\ell-nM] = K/M\delta[n]$. (Such $q[\ell]$ are often said to be self-orthogonal [3].) The term γ_p is a two-norm measure, and $\tilde{\gamma}_p$ is a one-norm measure.

D. Imaging of Subband Errors in the Output

The remaining performance measure of the filterbank captures the extent to which errors between the desired and actual outputs of the mth subband adaptive filter corrupt the filterbank output in other subbands. To be more precise, let $R_m(z)$ denote the (z-transform of the) desired output of the mth subband adaptive filter. The error signal that drives that adaptive filter is $\tilde{E}_m(z) = R_m(z) - \tilde{S}_m(z)$; see also Fig. 7 in Section VI. Such errors naturally manifest themselves in the mth subband of the output. However, images of $\tilde{E}_m(z)$ also appear outside the mth subband of the output. If we let $\tilde{\Omega}_M^m = \{\omega : \alpha_m - \pi/M \leq \omega \leq \alpha_m + \pi/M\}$ denote the mth subband of the output, then the energy of the imaged components of $\tilde{E}_m(z)$ is

$$E_{I_m} = \frac{1}{2\pi} \int_{(-\pi,\pi]\setminus\tilde{\Omega}_M^m} |G_m(e^{j\omega})\tilde{E}_m(e^{jK\omega})|^2 d\omega.$$

If we let $U_{\tilde{E}_m} \triangleq \max_\omega |\tilde{E}_m(e^{j\omega})|$, then

$$\begin{aligned} E_{I_m} &\leq \frac{U_{\tilde{E}_m}^2}{2\pi} \int_{\pi/M}^{2\pi-\pi/M} \left|P(e^{j\phi})\right|^2 d\phi \\ &= U_{\tilde{E}_m}^2 \left(E_{P,\mathrm{tb}} + E_{P,\mathrm{sb}}\right) \end{aligned}$$

where $E_{P,\mathrm{tb}} = (1/\pi)\int_{\pi/M}^{\pi/K} |P(e^{j\omega})|^2 d\omega$ is the energy in the transition band of the prototype filter, and $E_{P,\mathrm{sb}}$ is the stopband energy.

IV. Prototype Design

As we have argued in the Introduction, the performance of subband adaptive filtering systems is sensitive to the error mechanisms discussed in Section III. Now that the extent of these error mechanisms for oversampled GDFT filterbanks has been bounded by simple functions of the prototype filter, we can design filters that optimize these bounds so that optimized subband signal processing systems can be realized. Using the analysis in Section III, it is clear that we have the following.

1) For a given normalization, small values of the maximum stopband level $U_{P,\mathrm{sb}}$, the stopband energy $E_{P,\mathrm{sb}}$, and the maximum spectral component U_P of the prototype filter will guarantee that the energy of the aliased components in the subbands and the output is small.
2) A small value of γ_p in (27) will guarantee that the energy of the (amplitude and phase) distortion in the output is small.
3) Small values of the transition-band energy $E_{P,\mathrm{tb}}$ and the stopband energy $E_{P,\mathrm{sb}}$ will guarantee that the energy of imaged subband errors in the output is small.

Although various combinations of some of these criteria have been employed by other authors (on a somewhat *ad hoc* basis), we have shown how they explicitly bound the energy of the aliased components in the subbands and the output, the energy of the distortion in the output, and the energy of the imaged subband errors in the output. A natural design criteria for the prototype can be obtained by minimizing a (linear) combination of $U_{P,\mathrm{sb}}$, $E_{P,\mathrm{sb}}$, U_P, γ_p, and $E_{P,\mathrm{tb}}$, subject to bounds on their individual values.

For example, we might wish to find the length L prototype filter that minimizes the stopband energy, subject to fixed bounds on the maximum stopband level, the distortion coefficient, the transition-band energy, and the maximum spectral component of the filter, subject to the filter being normalized. That is, we might seek the solution of the following optimization problem:

$$\min_{\substack{p[\ell] \\ 0\leq\ell\leq L-1}} \quad \frac{1}{2\pi}\int_{\pi/K}^{2\pi-\pi/K} \left|P(e^{j\omega})\right|^2 d\omega \tag{29a}$$

$$\text{subject to} \quad \left|P(e^{j\omega})\right| \leq \epsilon_{\mathrm{sb}} \quad \forall\, \omega \in \left[\frac{\pi}{K}, \pi\right] \tag{29b}$$

$$\sum_{\substack{n \\ n\neq 0}} \left|\sum_{\ell} p[\ell]p[\ell - Mn]\right|^2 \leq \epsilon_\gamma^2 \tag{29c}$$

$$\frac{1}{\pi}\int_{\pi/M}^{\pi/K} \left|P(e^{j\omega})\right|^2 d\omega \leq \epsilon_{\mathrm{tbe}} \tag{29d}$$

$$\left|P(e^{j\omega})\right| \leq B \quad \forall\, \omega \tag{29e}$$

$$\sum_{\ell} p[\ell]^2 = \frac{K}{M} \tag{29f}$$

where ϵ_{sb}, ϵ_γ^2, ϵ_{tbe}, and B are fixed constants. Note that in contrast to standard peak-constrained least-squares filter design [39], the design criteria do not include an explicit lower bound on the magnitude spectrum in the passband of the prototype filter. However, by generalizing Nyquist's first criterion for intersymbol-interference-free pulse amplitude modulation, it can be shown that the distortion and maximum stopband level constraints [(29b) and (29c), respectively] implicitly control the pass-band "ripple" [34, App. A].

The integrals in (29a) and (29d) can be analytically evaluated, resulting in a convex quadratic objective and a convex quadratic constraint, respectively, and by squaring both sides of (29b) and (29e), we obtain two infinite sets of convex quadratic constraints (each expression generates one constraint for each relevant frequency). These infinite sets of constraints can be approximated by discretization [40]. [A simple discretization scheme is discussed in (31) below.] Therefore, in the absence of (29c), the problem in (29) could be efficiently solved, using, for example, second-order cone programming techniques [41]. Unfortunately, the distortion constraint in (29c) is, in general, a nonconvex quadratic function of $p[\ell]$. Hence, the problem in (29) is a nonconvex optimization problem that may require careful (and computationally expensive) management of locally optimal solutions in order to obtain a filter whose performance is sufficiently close to that of a globally optimal filter. This is important because the objective and the constraints in (29) are competing criteria. For example, it is well known that there is a tradeoff between the maximum stopband level and the stopband energy (e.g., [39]). Achieving a good design involves an exploration of the tradeoffs between these criteria, followed by the design of a filter that achieves a desired position on the tradeoff surface. The nonconvexity of (29) can make it quite awkward to get an accurate description of the tradeoff surface and, hence, quite difficult to determine how far a given filter is from providing an optimal tradeoff. Furthermore, it can be quite awkward to determine when the constraints in (29) conflict so that there is no filter of the given length that satisfies all the constraints, i.e., reliable detection of infeasibility of (29) can be difficult to achieve.

Given the difficulties involved in solving (29), some authors have developed interesting approximations to the distortion measure (29c), such as considering only amplitude distortion and ignoring phase distortion [22]. Others have simplified the design by iteratively linearizing $\sum_\ell p[\ell]p[\ell - Mn]$ and employing the iterative least squares technique to determine (locally) optimal filters for the simplified formulation [19]. (The method in [19] will be discussed in more detail in Section VI.) In contrast, the proposed method solves (29) without approximation or additional constraints and allows efficient and accurate calculation of the design tradeoffs and filters that achieve them.

The key observation in the development of the proposed design method is that the objective and the constraints in (29) are all convex functions of the autocorrelation of the filter coefficients

$$r_p[n] = \sum_\ell p[\ell]p[\ell - n].$$

Using the fact that $r_p[-n] = r_p[n]$ and $R_p(e^{j\omega}) = |P(e^{j\omega})|^2 = r_p[0] + 2\sum_{n\geq 1} r_p[n]\cos(\omega n)$, the integrals in (29a) and (29d) can be analytically evaluated. They are equal to $\sum_{n\geq 0} b_s[n]r_p[n]$ and $\sum_{n\geq 0} b_t[n]r_p[n]$, respectively, where $b_s[0] = 1 - 1/K$, $b_s[n] = -2\sin(\pi n/K)/(\pi n)$ for $n \geq 1$, $b_t[0] = 1/K - 1/M$, and $b_t[n] = 2(\sin(\pi n/K) - \sin(\pi n/M))/(\pi n)$ for $n \geq 1$. Therefore, the design problem in (29) can be transformed into the following optimization problem in $r_p[n]$, $n \geq 0$:

$$\min_{\substack{r_p[n] \\ 0\leq n\leq L-1}} \quad \sum_{n\geq 0} b_s[n]r_p[n] \tag{30a}$$

$$\text{subject to} \quad R_p(e^{j\omega}) \leq \epsilon_{\text{sb}}^2, \quad \forall\, \omega \in \left[\frac{\pi}{K}, \pi\right] \tag{30b}$$

$$\sum_{i\geq 1} r_p[Mi]^2 \leq \frac{\epsilon_\gamma^2}{2} \tag{30c}$$

$$\sum_{n\geq 0} b_t[n]r_p[n] \leq \epsilon_{\text{tbe}} \tag{30d}$$

$$R_p(e^{j\omega}) \leq B^2, \quad \forall\, \omega \tag{30e}$$

$$r_p[0] = \frac{K}{M} \tag{30f}$$

$$R_p(e^{j\omega}) \geq 0, \quad \forall\, \omega. \tag{30g}$$

This change of variables must be handled carefully because not all sequences $r_p[n]$ are the autocorrelation coefficients of some filter. A necessary and sufficient condition for $r_p[n]$ to correspond to the autocorrelation coefficients of a filter is (30g), e.g., [42]. Given a sequence $r_p[n]$ that solves (30), filter coefficients $p[\ell]$ that generate this autocorrelation can be found using standard spectral factorization techniques [30], [35].

The objective in (30a) and the constraints in (30b) and (30d)–(30g) are linear, and hence convex, in $r_p[n]$, $0 \leq n \leq L-1$, and (30c) is a convex quadratic constraint.[4] Therefore, the tradeoffs between these competing prototype design criteria can be efficiently evaluated and an optimal autocorrelation efficiently found using convex optimization techniques. Furthermore, infeasibility of (30) can be reliably detected.

Unfortunately, the constraints in (30b), (30e), and (30g) each generate an infinite number of linear constraints on $r_p[n]$—one for each relevant frequency—and it may appear that these could be awkward to handle in practice. One possible approach is to approximate the constraints by discretization [40]. A simple scheme for discretizing (30b) is to choose a set of frequencies $\pi/K \leq \omega_1 \leq \omega_2 \leq \cdots \leq \omega_N \leq \pi$, which are often uniformly spaced, and approximate (30b) with N ordinary inequality constraints

$$R_p(e^{j\omega_k}) \leq \epsilon_{\text{sb}}^2 - \epsilon_N, \quad k = 1, 2, \ldots, N \tag{31}$$

where ϵ_N is chosen heuristically so that satisfaction of (31) guarantees satisfaction of (30b). In this way, the design problem can be approximated by a finite-dimensional problem with linear and convex quadratic constraints—a problem that is efficiently solvable, using, for example, second-order cone programming techniques [41]. As the number of discretization points N is increased, ϵ_N can be reduced, and hence, the quality of the approximation improves. However, this also increases the number of constraints in the optimization problem, which may result in longer solution times and may expose the problem to numerical difficulties. A "rule of thumb" is that $N \geq 15L$ will provide a sufficiently accurate approximation [30].

An elegant, precise, and finite-dimensional alternative to discretizing these linear constraints is to transform them into linear matrix inequalities (LMIs)[31], which can be efficiently enforced using semidefinite programming (SDP) techniques [43]. In the case of (30g), we can exploit the positive real lemma, which states (e.g., [31]) that $R_p(e^{j\omega}) \geq 0$, $\forall\, \omega$ if and only if there exists a symmetric positive semidefinite matrix $\boldsymbol{X}_1 \in \mathbb{R}^{L\times L}$ such that

$$\sum_{k=0}^{L-1-n} [\boldsymbol{X}_1]_{k,k+n} = r[n], \quad n = 0, 1, \ldots, L-1 \tag{32}$$

where $[\cdot]_{ij}$ denotes the (i,j)th element of a matrix. (A symmetric matrix is said to be positive semidefinite if all its eigenvalues are non-negative. This will be denoted by $\boldsymbol{X}_1 \geq \boldsymbol{0}$.) Similarly, we can use the bounded real lemma (e.g., [31]) to enforce (30e): $R_p(e^{j\omega}) \leq B^2$, $\forall\, \omega$, if and only if there exists a symmetric positive semidefinite matrix $\boldsymbol{X}_2 \in \mathbb{R}^{L\times L}$ such that

$$\sum_{k=0}^{L-1-n} [\boldsymbol{X}_2]_{k,k+n} = B^2\delta[n] - r_p[n], \quad n = 0, 1, \ldots, L-1. \tag{33}$$

Equations (32) and (33) are finite sets of linear constraints on the semidefinite matrix $\boldsymbol{X}_i$ and are (exactly) equivalent to the infinite set of linear constraints on $r_p[n]$ generated by (30e) and (30g), respectively. Similarly, for the maximum stopband level constraint $R_p(e^{j\omega}) \leq \epsilon_{\text{sb}}^2$, $\forall\, \omega \in [\pi/K, \pi]$ if and only if [31] there exist positive semidefinite matrices $\boldsymbol{X}_3 \in \mathbb{R}^{L\times L}$ and $\boldsymbol{Z} \in \mathbb{R}^{(L-1)\times(L-1)}$ such that

$$(2 - \delta[n])x_{\text{sd}}[n] + q[n] = \left(\epsilon_{\text{sb}}^2 + r[0]\right)\delta[n] - 2r_p[n] \tag{34}$$

where we have (35)–(37), shown at the bottom of the next page, $d_0 = 2(\cos(\pi/K) - \cos^2(\pi/K))$ and $d_1 = 2(\cos(\pi/K) - 1)$.

[4]For reasons of numerical accuracy, one may wish to replace (30c) by $\left(\sum_{i\geq 1} r_p[Mi]^2\right)^{1/2} \leq \epsilon_\gamma/\sqrt{2}$, which is a (convex) second-order cone constraint [41].

This LMI approach has the advantage that the transformation to the finite problem is precise, and hence, we avoid having to select N and ϵ_N in (31). The resulting optimization problems can be expressed as

$$\min_{r_p[n],\boldsymbol{X}_1,\boldsymbol{X}_2,\boldsymbol{X}_3,\boldsymbol{Z}} \quad \sum_{n\geq 0} b_s[n]r_p[n] \tag{38a}$$

$$\text{subject to} \quad \boldsymbol{X}_1 \geq \boldsymbol{0}, \quad \boldsymbol{X}_2 \geq \boldsymbol{0} \quad \boldsymbol{X}_3 \geq \boldsymbol{0}, \quad \boldsymbol{Z} \geq \boldsymbol{0} \tag{38b}$$

$$(32)\text{-}(34),\ (30c),\ (30d),\ \text{and}\ (30f). \tag{38c}$$

The problem in (38) is a (convex) cone program with a combination of linear, second-order, and semidefinite cones and can be efficiently solved using general-purpose solvers for such problems (e.g., [44]). Furthermore, there are some early indications (e.g., [45]) that the inherent structure in (38) can be exploited using specially designed algorithms that are substantially more efficient than general-purpose methods.

V. Design Tradeoffs

In this section, we illustrate how the proposed convex formulation in (38) can be used to efficiently evaluate the tradeoffs in prototype filter design for oversampled NPR GDFT filterbanks. As discussed in the Introduction, an important tradeoff is that between aliasing in the subbands and the distortion induced by the filterbank. In Section III, we showed that the energy of the aliased components in the subbands can be bounded by linear functions of the maximum stopband level and the stopband energy of the filter and that these two quantities, along with the maximum spectral component of the filter, bound the energy of the aliased components at the output. In addition, we showed that the energy of the distortion error induced by the filterbank can be bounded by a multiple of the distortion coefficient γ_p^2 [see (26)]. Therefore, a natural tradeoff to explore is how the minimum achievable stopband energy varies with the bound on the distortion coefficient ϵ_γ^2 for a given bound on the maximum stopband level (and a fixed bound on the maximum spectral component and the transition-band energy). This tradeoff can be efficiently obtained by solving (38) [or a discretized version of (30)] for different values of ϵ_γ^2 and fixed values of ϵ_{sb}^2, B^2 and ϵ_{tbe}. The resulting tradeoff curve generates considerable insight into the design of the prototype filter, as we illustrate in the following example.

Example 1: Consider a GDFT filterbank with $M = 8$ subbands and a down-sampling factor of $K = 6$. As in Section III-C, we normalize the prototype to have energy $\sum_\ell p[\ell]^2 = K/M$. To make an appropriate choice for the upper bound on the maximum spectral component B, we observe that if the stopband suppression is substantial, then most of the filter's energy lies in the passband $\omega \in [0, \pi/M]$. Using Parseval's relation, in order for the prototype to have energy K/M, the average value of $|P(e^{j\omega})|^2$ over this band must be around K. Since $K = 6$ in this example, this is around 7.8 dB. To allow for some variation of the spectrum over the passband, we set $B^2 = 10^{0.1}K$, i.e., around 8.8 dB. The tradeoff between the minimum achievable stopband energy and the bound on the distortion coefficient for certain maximum allowable stopband levels for filters of length 48 is given in Fig. 3.[5] (As discussed below, the constraint on the transition-band energy was not activated in this example.) These curves represent the *inherent* tradeoff between the stopband energy and the distortion coefficient because all points on or above (and to the right of) the curves can be achieved with a length 48 filter, and no length 48 filter can achieve any point below (and to the left of) the curves. Each point on these curves was found by solving (38) using the `SeDuMi` toolbox [44] for MATLAB.[6] This task required between 3 and 6 s of CPU time on a 1.6-GHz Pentium IV workstation. The power spectra of three representative filters are given in Fig. 4, along with the corresponding masks. From Fig. 3, we can see that when considerable distortion is allowed, the maximum stopband level constraints we have chosen are inactive. (The tradeoff curves coalesce.) However, as the distortion constraint is made more stringent, the maximum stopband level constraints become active. In fact, when the maximum stopband level constraint is 34.5 or 36 dB below the maximum spectral component constraint, there is no length 48 filter that satisfies this constraint and has a vanishingly small distortion coefficient. (The achievable regions for these constraints, indicated by the dashed and dash-dot curves, respectively, are bounded on the left.) Note, also, that a stopband energy "floor" is encountered when considerable distortion is allowed. This

[5]The filter length is chosen to be an integer multiple of $M/2$ for compatibility with the competing interpolation-based method described in Section VI. The proposed design method does not place any constraints on the filter length. Length 49 filters for this example were designed in [46].

[6]A MATLAB "m-file" that expresses (38) in the input format required by `SeDuMi` is available from the second author's web site at http://www.ece.mcmaster.ca/~davidson.

$$x_{\text{sd}}[n] = \sum_{k=0}^{L-1-n} [\boldsymbol{X}_3]_{k,k+n}, \quad n = 0, \ldots, L-1 \tag{35}$$

$$q[n] = \begin{cases} d_0 z_{\text{sd}}[0] + d_1 z_{\text{sd}}[1], & n = 0 \\ 2d_0 z_{\text{sd}}[n] + d_1 z_{\text{sd}}[n-1] + d_1 z_{\text{sd}}[n+1], & n = 2, \ldots, L-3 \\ 2d_0 z_{\text{sd}}[L-2] + d_1 z_{\text{sd}}[L-3], & n = L-2 \\ d_1 z_{\text{sd}}[L-2], & n = L-1 \end{cases} \tag{36}$$

$$z_{\text{sd}}[n] = \sum_{k=0}^{L-2-n} [\boldsymbol{Z}]_{k,k+n}, \quad n = 0, \ldots, L-2 \tag{37}$$

floor is due to the maximum spectral component constraint (30e).

Given the proximity of π/M and π/K in this example, compatible constraints on the transition-band energy have only marginal effects on Fig. 3. More precisely, the range of transition-band energy constraints that are active and result in the optimization problem having a nonempty feasible set is rather narrow. Hence, the corresponding curves have been omitted from Fig. 3 for clarity. (This decision is validated by Table I in Section VI.) However, in Section VI, we will show that constraints on the transition-band energy have a considerable impact when the filterbank has a downsampling factor of $K = 4$ rather than $K = 6$. □

A distinct advantage of the design method developed in this paper is its flexibility. Many other inherent design tradeoffs can be explored using simple modifications to the design problem in (38). For example, we can determine how the minimum achievable maximum stopband level varies with the bound on the distortion coefficient for a given bound on the stopband energy by simply replacing the objective in (38) by $\epsilon_{\rm sb}^2$ and by introducing the additional linear constraint $\sum_{n\geq 0} b_s[n]r_p[n] \leq \epsilon_{\rm sbe}$. As one might expect, the general trend of the resulting tradeoff curves is similar to that in Fig. 3, but quantifying this trend remains an important task in practice; see [47] for further details.

Another interesting tradeoff is that between the minimum achievable stopband energy and the maximum allowable stopband level for a given bound on the distortion coefficient. Curves of this type are often encountered in peak-constrained least-squares filter design [39] but usually without the distortion constraint. We can efficiently evaluate this tradeoff by simply solving (38) for a range of values of $\epsilon_{\rm sb}^2$ given fixed values of ϵ_γ^2 and B^2; see [47] for an example. The resulting tradeoff curves indicate that relatively mild constraints on the distortion coefficient have a considerable impact on the stopband energy/stopband level tradeoff but that as the distortion constraint becomes more stringent, the impact of changes in this constraint is significantly reduced.

An auxiliary problem that arises in filterbank design is the choice of the length of the prototype filter. Typically, for complexity reasons, we would like to use the shortest prototype that satisfies a given performance level. Finding this minimum-length prototype can be quite awkward using the nonconvex formulation in (29) because it can be quite difficult to determine whether or not a given set of constraints generates a nonempty feasible set. In contrast, infeasibility of the proposed convex formulation [(30) or (38)] can be reliably detected. Therefore, the shortest length that achieves a given specification can be efficiently determined using a bisection-based search (on the filter length) for the feasibility boundary of a modified version of (30) [or (38)] in which the objective is removed, and the linear constraint $\sum_{n\geq 0} b_s[n]r_p[n] \leq \epsilon_{\rm sbe}$ is added. (An analogous procedure in a different application appears in [48].) We illustrate that procedure in the following example.

Example 2: In Example 1, we examined the tradeoff between the minimum achievable stopband energy and the distortion coefficient for prototype filters of length 48. Using the above-mentioned bisection search method, we found that the shortest filters achieving the tradeoff denoted by the ★ in Fig. 3 for maximum stopband levels 0, 30, 33, 34.5, and 36 dB below the maximum spectral component constraint are of lengths 36, 42, 44, 48, and 49, respectively. Notice that the last case requires a filter longer than 48. This is what we would expect, because the ★ lies outside the corresponding achievable region for length 48 filters. □

As we have seen in this section, a feature of the proposed design approach is that it is universal in the sense that the tradeoff curves can be obtained without knowledge of the application nor of the input signal. However, selection of an appropriate point on the resulting tradeoff surface depends on the relative importance of the three error mechanisms (aliasing in the subbands and the output, distortion, and imaging in the output) on the application at hand, as well as on the properties of the input signal. While the selection of that point will require a certain amount of application-specific empirical performance evaluation, the bounds derived in Section III provide some guidance as to how the properties of the input signal affect the relative importance of a small stopband energy, a small maximum stopband level, a small distortion coefficient, and a small transition-band energy. For example, the signal-dependent coefficients of the bound on the aliasing in the subbands in (15) and the bound on the distortion in (26) are quite different. If these two error mechanisms are of equal importance in a given application, then for a given signal, the relative sizes of the signal-dependent coefficients will guide the designer toward a point on the maximum stopband level versus distortion coefficient tradeoff curve that is appropriate for that signal.

VI. Performance Comparison

Now that we have provided examples of the inherent tradeoffs in prototype filter design and have shown that the proposed design method provides filters that achieve these tradeoffs, we will compare the proposed method with two competing methods [19], [20]. Both methods are of interest because, like the proposed method, they generate filterbanks with nearly paraunitary polyphase matrices, and they tackle the distortion induced by the filterbank directly. In contrast, many other methods employ approximations of the distortion, such as considering only amplitude distortion [22].

The method proposed by Harteneck *et al.* [19] (see also [16]) involves minimizing a linear combination of the stopband energy $E_{P,\rm sb}$, the distortion coefficient γ_p^2, and any normalization error, subject to the prototype filter having linear phase. In the notation of the present paper, this can be written as

$$\min_{\substack{p[\ell]\\ 0\leq\ell\leq L-1}} \quad \lambda E_{P,\rm sb} + \gamma_p^2 + \left(\sum_\ell p[\ell]^2 - \frac{K}{M}\right)^2 \tag{39a}$$

$$\text{subject to} \quad P(e^{j\omega}) \text{ having linear phase} \tag{39b}$$

where $\lambda \geq 0$ is a chosen weighting. For symmetric filters, imposing phase linearity is equivalent to requiring $p[\ell] = p[L-1-\ell]$. The problem in (39) is not convex and, hence, may require delicate management of local minima. However, given a linear-phase filter as a "starting point," a local minimum can be found quite efficiently using an iterative least-squares (ILS)

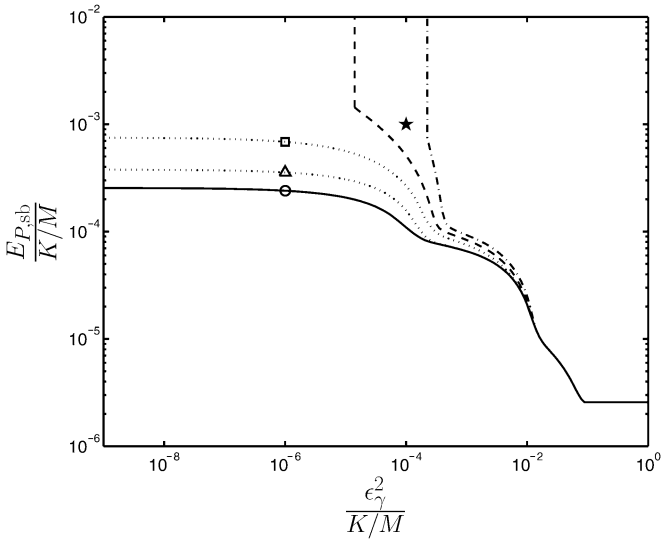

Fig. 3. Tradeoff between the fraction of the total filter energy that is in the stopband $E_{P,\mathrm{sb}}/(K/M)$ and the (normalized) bound on the distortion coefficient $\epsilon_\gamma^2/(K/M)$ for length 48 filters with maximum stopband levels 0 dB (solid), 30 dB (dotted with $\triangle$), 33 dB (dotted with $\square$), 34.5 dB (dashed), and 36 dB (dash-dot) below the maximum spectral component constraint. The symbols $\circ$, $\triangle$, and $\square$ denote the tradeoffs achieved by the filters in Fig. 4(a)–(c), respectively. The point denoted by the $\bigstar$ is used in Example 2.

technique [27]. In our implementation, we ran the ILS algorithm from several systematic starting points and several random starting points and then chose the locally optimal filter with the lowest objective as our solution. Our systematic starting points included the length-L truncation of the square-root raised cosine filter (e.g., [28, p. 496]) with cut-off frequency π/M and roll-off parameter $(M/K) - 1$.

Although our analysis (see Section III) and some simulations (below) suggest that our standard formulation [(29), (30), or (38)] is more appropriate for many subband processing applications, we can obtain a convex problem similar to that in (39) by simply dropping the maximum stopband level, transition-band energy, and maximum spectral component constraints [(30b), (30d) and (30e), respectively] from (30) and lifting the distortion constraint (30c) into the objective

$$\min_{r_p[n],\tau_1,\tau_2} \quad \lambda\left(\sum_{n\geq 0} b_s[n]r_p[n]\right) + \tau_1 + \tau_2 \tag{40a}$$

$$\text{subject to} \quad \sum_{i\geq 1} r_p[Mi]^2 \leq \frac{\tau_1}{2} \tag{40b}$$

$$\left(r_p[0] - \frac{K}{M}\right)^2 \leq \tau_2 \tag{40c}$$

$$R_p(e^{j\omega}) \geq 0, \quad \forall\, \omega. \tag{40d}$$

Here, τ_1 is the appropriate bound on the distortion coefficient γ_p^2, and τ_2 is the bound on the normalization error. As discussed in Section IV, the third constraint (40d) can be handled via discretization or via transformation into an LMI. Notice, however, that we do not impose the phase linearity constraint in (40) or in any of our other formulations.

In contrast to the optimization-based methods proposed by Harteneck *et al.* [19] and herein, Liu *et al.* [20] proposed

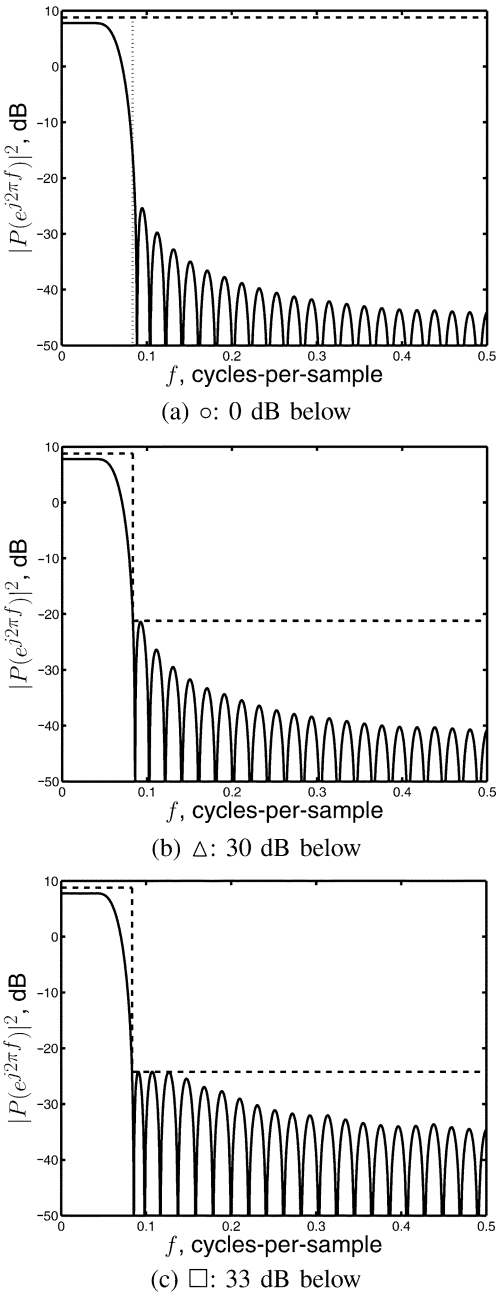

(a) $\circ$: 0 dB below

(b) $\triangle$: 30 dB below

(c) $\square$: 33 dB below

Fig. 4. Power spectra (in decibels) of filters that achieve the stopband energy versus distortion coefficient tradeoff curve in Fig. 3 for a distortion coefficient of $10^{-6}\,\mathrm{K/M}$ and maximum stopband level constraints 0, 30, and 33 dB below the maximum spectral component constraint. For clarity, the spectral mask imposed by the maximum spectral component and maximum stopband level constraints is shown by the dashed line. (a) We have also indicated the stopband edge $1/(2K)$ with a dotted line. (b) and (c) This edge is clear from the mask.

a simple, but *ad hoc*, method based on interpolated filters [49], [50]. To obtain a "good" prototype filter, Liu *et al.* [20] suggest that one can simply interpolate the lowpass filter from an orthonormal two-channel filterbank by a factor of $M/2$. There are many well-known constructions of such filterbanks [2]–[4], [51] and many choices for the interpolation algorithm. As suggested by Liu *et al.* [20], we will use MATLAB's `interp` function to perform the interpolation. (While that choice does provide "good" interpolation, the interpolation depends on the filter from the two-channel filterbank.) We will

TABLE I
STEADY-STATE MEAN SQUARE ERROR (SS-MSE) FOR THE ADAPTIVE FILTERING SYSTEM IN EXAMPLE 4 EQUIPPED WITH PROTOTYPE FILTERS FROM EXAMPLE 3 (SEE FIG. 5). ALSO INCLUDED ARE THE NORMALIZED DISTORTION COEFFICIENT (γ_p^2/E_p), THE MAXIMUM RELATIVE STOPBAND LEVEL BELOW $B^2 = 10^{0.1}K$ (REL. SBL), AND THE NORMALIZED STOPBAND ($E_{P,\mathrm{sb}}/E_p$) AND TRANSITION-BAND ($E_{P,\mathrm{tb}}/E_p$) ENERGIES

Design Method	Symbol in Fig. 5	γ_p^2/E_p,	rel. SBL, dB	$E_{P,\mathrm{sb}}/E_p$, $\times 10^{-4}$	$E_{P,\mathrm{tb}}/E_p$ $\times 10^{-2}$	SS-MSE, dB
Harteneck [19]	▶	10^{-8}	-20.0	17.4	6.24	-20.02
Proposed, no mask, (41)	⊕	10^{-8}	-24.5	2.54	5.62	-23.05
Proposed (38)	⊠	10^{-8}	-30.0	3.76	5.26	-23.42
Proposed (38)	⊞	10^{-8}	-33.0	7.44	5.02	-22.74
Harteneck [19]	◀	10^{-6}	-20.6	9.06	6.20	-21.29
Proposed, no mask, (41)	○	10^{-6}	-24.6	2.40	5.57	-23.11
Proposed (38)	△	10^{-6}	-30.0	3.55	5.23	-23.46
Proposed (38)	□	10^{-6}	-33.0	6.86	5.00	-22.88
Harteneck [19]	▼	10^{-4}	-22.01	4.66	5.88	-22.14
Proposed, no mask, (41)	●	10^{-4}	-26.6	1.09	5.06	-23.75
Proposed (38)	▲	10^{-4}	-30.0	1.57	4.91	-23.97
Proposed (38)	■	10^{-4}	-33.0	2.68	4.78	-23.91
Harteneck [19]	♦	10^{-3}	-23.6	2.82	5.21	-21.89
Proposed, no mask, (41)	⊗	10^{-3}	-30.0	0.65	4.27	-23.07
Proposed (38)		10^{-3}	-33.0	0.75	4.12	-23.27
Interp. [20], MSB [52],[53]	$*$	2.08×10^{-3}	-14.3	82.8	8.45	-15.52
Interp. [20], Daubech. [51]	$+$	1.02×10^{-4}	-16.9	26.6	6.96	-19.66
Interp. [20], symlet [51]	$\times$	2.14×10^{-5}	-15.9	21.0	7.04	-20.53

restrict attention to interpolations of lowpass filters from the standard Daubechies family [51] of orthonormal two-channel filterbanks, the symlet family [51], and those obtained from "windowed" ideal autocorrelations [52], [53]. We will choose the minimum-phase spectral factor for the window-based designs and will denote them by "MSB." After evaluating the performance of the standard data analysis windows [54], we found that the "Blackmann–Harris" window [54, p. 65] is an appropriate choice for the application at hand.

In the following example, we demonstrate how the proposed formulations can provide prototype filters with significantly better design tradeoffs than those generated by Harteneck's method and those generated by interpolation.

Example 3: In this example, we again consider a filterbank with $M = 8$, $K = 6$, and length 48 filters. In Fig. 5, we provide (with a dashed curve) the locus of normalized distortion coefficient-stopband energy pairs (γ_p^2/E_p, $E_{P,\mathrm{sb}}/E_p$) achieved by Harteneck's method [19] for different values of λ in (39). Here, $E_p = \sum_\ell p[\ell]^2$ is the energy of the filter. For clarity, we have indicated the points achieved by Harteneck's method for specific values of λ by the symbols on the dashed curve in Fig. 5. As one would expect, increasing λ moves the achieved tradeoff toward the bottom-right corner of the figure. Fig. 5 also contains the tradeoff points achieved by interpolation of filters from certain standard orthonormal two-channel filterbanks and the inherent tradeoff (achieved by the proposed method) between the stopband energy and the distortion coefficient (indicated by the solid

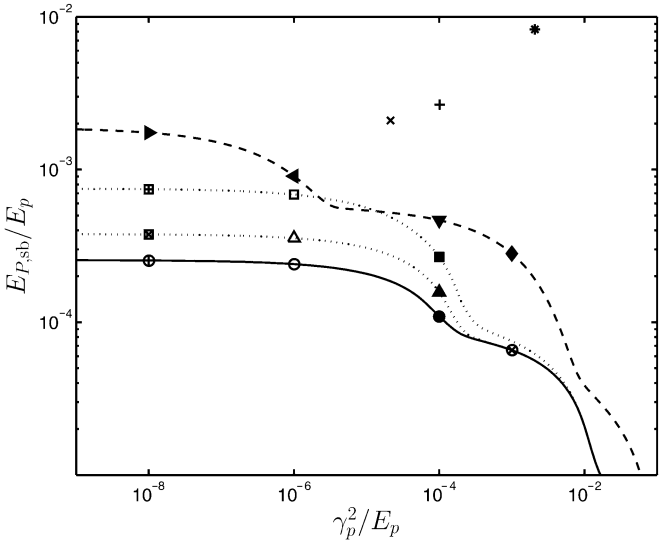

Fig. 5. Tradeoffs between the normalized stopband energy $E_{P,\mathrm{sb}}/E_p$ and the normalized distortion coefficient γ_p^2/E_p for Example 3. Solid: inherent tradeoff [achieved by the proposed method, (41)]; dashed: tradeoff achieved by Harteneck's method [19]; dotted: tradeoff achieved by the proposed method with additional constraints on the maximum spectral component and the maximum relative stopband level (38). Dotted with ⊠, △, and ▲: relative stopband level is -30 dB; dotted with ⊞, □, and ■: relative stopband level is -33 dB. (The solid and dotted curves coincide with the corresponding curves in Fig. 3.) The symbols ▶, ◀, ▼, and ♦ indicate the tradeoffs achieved by Harteneck's method with $\lambda = 8.86 \times 10^{-3}$, 3.91×10^{-2}, 1.01, and 2.09, respectively. The symbols $+$, $\times$, and $*$ denote the tradeoffs achieved by interpolating length-12 Daubechies, symlet, and MSB filters, respectively.

curve). To obtain the inherent tradeoff, we solved an LMI version of the problem:

$$\min_{r_p[n]} \quad \sum_{n\geq 0} b_s[n] r_p[n] \tag{41a}$$

$$\text{subject to} \quad \gamma_p^2 \leq \frac{\alpha K}{M}, \quad r_p[0] = \frac{K}{M}$$

$$R_p(e^{j\omega}) \geq 0, \quad \forall\, \omega \tag{41b}$$

for a range of values of α. Over the range of distortion coefficients in Fig. 5, the solid curve coincides with the solid curve in Fig. 3. (Note that for clarity the scale of Fig. 5 is slightly different from that in Fig. 3.) However, when greater distortion is allowed, the solid curve in Fig. 5 does not exhibit the floor effect seen on the right of Fig. 3 because (41) does not contain a constraint on the maximum spectral component. For reference, we have also incorporated the dotted curves from Fig. 3 into Fig. 5. These curves correspond to the stopband energy versus distortion tradeoff subject to bounds on the maximum spectral component and the maximum relative stopband level and were obtained by solving (38). The power spectra of representative filters are provided in Fig. 6. (We selected the interpolated symlet [symbol $\times$] rather than the interpolated Daubechies' filter [symbol $+$] because it achieves a superior tradeoff.) In addition, the power spectra of filters that achieve the tradeoffs denoted by the $\circ$, $\triangle$, and $\square$ in Fig. 5 are given in Fig. 4.

It is clear from Fig. 5 that by optimizing the prototype and avoiding the phase linearity constraint, the proposed method provides a significantly better tradeoff between stopband energy and distortion.[7] In particular, the dotted curves in Fig. 5 denote the stopband-energy versus distortion coefficient tradeoff achieved by filters that must also satisfy rather stringent spectral masks. Despite the fact that these filters satisfy this additional constraint, for a given distortion coefficient, they (almost always) achieve a lower stopband energy than the filter designed using Harteneck's method. $\square$

To verify that the improved tradeoffs achieved by the proposed method in Example 3 (see Fig. 5) can generate significant performance gains for the subband signal processing system as a whole, we now examine the performance of the simple subband adaptive filtering system illustrated in Fig. 7. The purpose of the subband adaptive filter (bounded by the dash-dot polygon in Fig. 7) is to approximate the impulse response of an unknown system $c[n]$. This configuration is often called a "system identification" configuration, as is commonly used in acoustic echo cancellation (AEC) applications [13]–[17], [20]–[22]. The subband adaptive filter operates by passing the (known) input signal $x[n]$ and noisy measurements $r[n]$ of the output of the unknown system through separate analysis filterbanks. (The sequence $v[n]$ denotes the noise.) The subband processing block is a diagonal matrix of standard adaptive filters, each of which operates (independently of the other filters) on one of the subband signals. (The elements that process the mth subband are enclosed in the dotted box in Fig. 7, where the dashed line indicates that the error signal $e_m[k]$ drives the adaptation of $w_m[i;k]$.) The filtered subband signals are then reconstructed, and as the filter converges, $y[n]$ approximates a delayed version of $r[n]$. Although Fig. 7 indicates that adaptive filtering is performed in every subband, if $x[n]$ and $c[n]$ are real, M is even, and if we insert a real part operator and a gain of two between the synthesis filterbank and the summer (i.e., if $e[n] = r[n-L+1] - 2\text{Re}(y[n])$), then we can perform adaptive filtering on only $M/2$ of the subbands and obtain the same performance [16], [17], [19]. If we choose $m_0 = 1/2$ in (1), we need only filter subbands $0 \leq m \leq M/2-1$. The resulting reduction in computational load has a significant impact in practice, and we will use this reduced-complexity system in the following simulations.

[7]Recall that the proposed method actually achieves the *inherent* tradeoff in the sense that no length 48 filter can achieve any point below the (solid) curve generated by the proposed method.

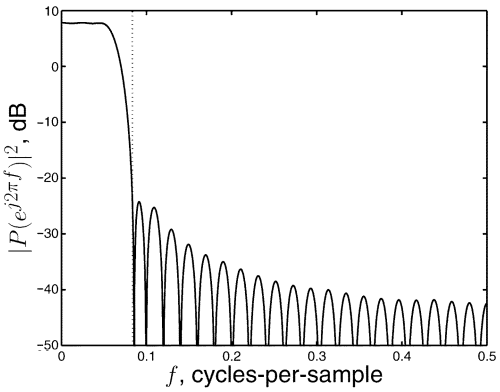

(a) ■: Proposed method (38)

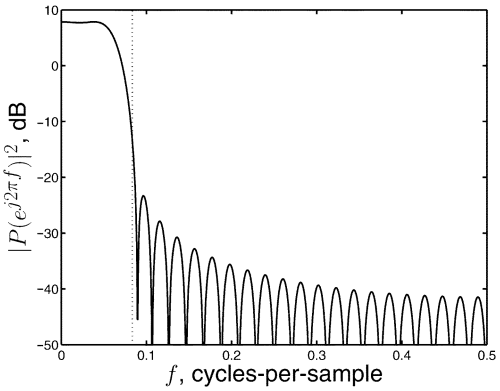

(b) ▼: Harteneck's method [19]

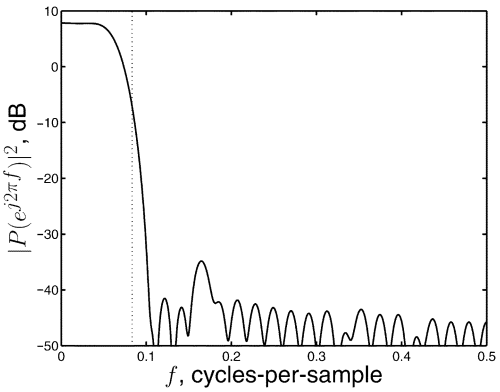

(c) $\times$: Interpolated symlet

Fig. 6. Power spectra (in decibels) of filters that achieve the stopband energy versus distortion coefficient tradeoffs indicated by the ■, ▼, and $\times$ in Fig. 5. For clarity, the stopband edge is indicated by the dotted line.

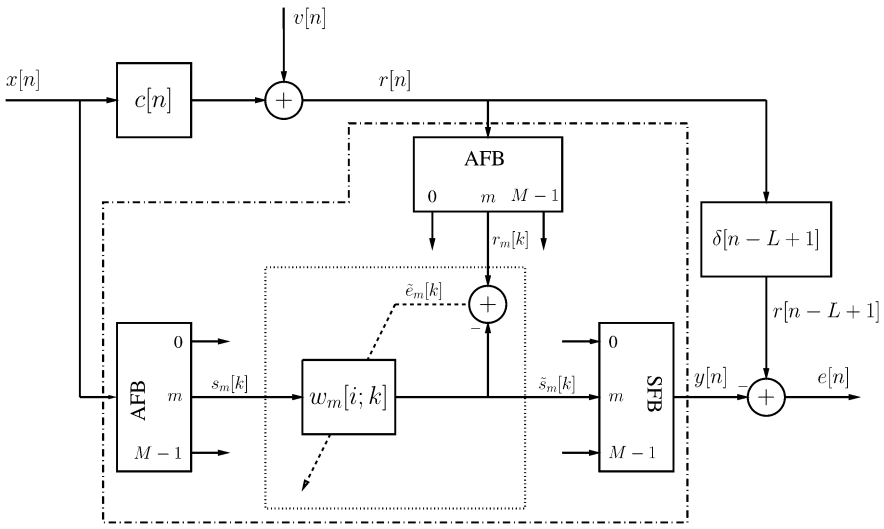

Fig. 7. Subband adaptive filtering system (enclosed by the dash-dot polygon) used in Example 4. For clarity, only one element of the (diagonal) subband processing block is shown (in the dotted box). The symbols AFB and SFB denote the analysis and synthesis filterbanks, respectively, $c[n]$ is the impulse response of the unknown system, and $w_m[i;k]$ is the impulse response of the adaptive filter in the mth subband at the kth instant.

Example 4: In this example, we examine the performance of the subband adaptive filter in Fig. 7 equipped with the GDFT filterbanks designed in Example 3 (see Fig. 5) in a synthetic acoustic echo cancellation (AEC) environment. Recall that the proposed method generates the optimal autocorrelation sequence from which an optimal filter can be obtained using standard spectral factorization techniques [30], [35]. For simplicity, we only report results for the minimum-phase spectral factor, but other experiments have indicated that in the scenario of this example, the performance variation over the different spectral factors tends to be small compared with the performance variations in Table I. In synthesizing the filterbanks from the prototype filter using (1), we chose $m_0 = 1/2$ so that we need only implement the adaptive filters in subbands $0 \leq m \leq 3$, and we chose $n_0 = -(L-1)/2 = 24$, so that if $p[n]$ has linear phase (as it does in Harteneck's designs), then all the filters $f_m[k]$ in the filterbank also have linear phase.

We evaluate the average performance of the subband adaptive filter over a class of randomly generated unknown systems $c[n]$ of length 60 whose impulse response coefficients tend to decay exponentially. More specifically, $c[n] \sim \mathcal{N}(0, e^{-n/10})$, $0 \leq n \leq 59$. This class of unknown systems shares many of the characteristics of the acoustic impulse response encountered in practical AEC applications. The adaptive filters $w_m[i;k]$ have length 10 and are adapted using the normalized least-mean square (NLMS) algorithm [55], with step-size coefficient $\tilde{\mu} = 0.8$. The input signal $x[n]$ is a (real) zero-mean white Gaussian signal of unit variance, and in order to isolate the performance of the filterbank, no noise was injected into the measured signal $r[n]$, i.e., $v[n] = 0$.

The steady-state mean square error (SS-MSE), averaged over 10 000 realizations of the unknown system and the input signal, for systems based on filters that achieve the marked tradeoffs in Fig. 5, is provided in Table I. For convenience, we have listed, in Table I, the (normalized) distortion coefficient, the relative stopband level, and the (normalized) stopband and transition-band energies of each filter. From Table I, it is clear that for a given distortion coefficient, the lower stopband and transition-band energies achieved by the simplest of the proposed formulations [which has no spectral mask (41)] result in a substantial improvement in the SS-MSE over that achieved by the corresponding interpolated filters, and a significant improvement over that achieved by the corresponding filter designed by Harteneck's method. Table I also shows that our standard formulation [(30) or (38)] with a mild constraint on the maximum stopband level results in further performance improvement. For example, the filter with the symbol ■ has

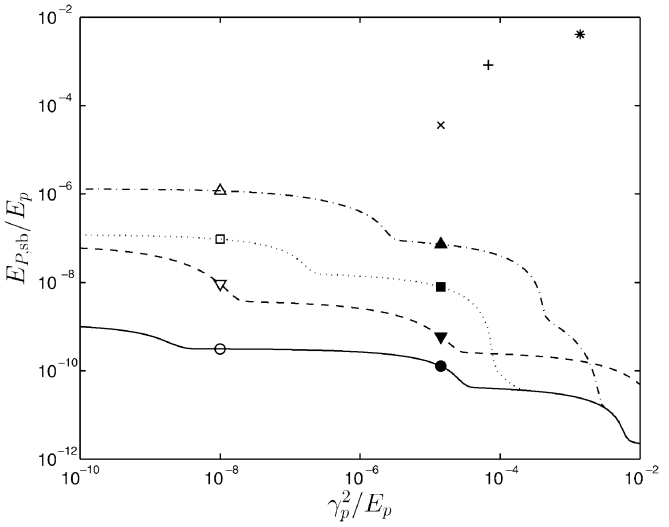

Fig. 8. Tradeoffs between the normalized stopband energy $E_{P,\mathrm{sb}}/E_p$ and the normalized distortion coefficient γ_p^2/E_p for Example 5. Legend—solid: proposed method, without a constraint on the transition-band energy (TBE); dashed: Harteneck's method [19]; other curves: proposed method with the TBE constrained to be less than ρ times that achieved by the interpolated symlet; dotted: $\rho = 1$; dash-dot: $\rho = 0.8$. The symbols $+$, $\times$, and $*$ denote the tradeoffs achieved by interpolated length-12 Daubechies, symlet, and MSB filters, respectively.

an SS-MSE that is around 3.4 dB lower than that of the interpolated symlet (symbol $\times$) and around 1.6 dB lower than that of the corresponding filter from Harteneck's method (symbol $\blacktriangledown$). However, if the maximum stopband level constraint is too stringent, and the resulting increase in the stopband and transition-band energies is too large, then the SS-MSE begins to increase. It can also be observed from Table I that as the distortion constraint is relaxed from $10^{-8}E_p$, the performance of the filters from each design method improves, but as this constraint becomes rather loose, the performance begins to degrade. Finally, Table I justifies our earlier decision (in Section V) to leave the transition-band energy constraint inactive for this scenario. Even without a specific transition-band energy constraint, the proposed method achieves a consistently lower transition-band energy than the competing methods. □

Although the steady-state mean square errors of the systems in Table I might be regarded as being rather high, and although the performance differences are quite subtle in places, Example 4 has validated the major principles of the proposed design approach. First, the performance of a GDFT-filterbank-based subband adaptive filtering system depends on the properties of the prototype filter that we derived in Section III, namely, the stopband energy, the maximum stopband level, the distortion coefficient, and the transition-band energy; and second, to obtain optimized performance from the subband adaptive filter in a particular application, we should explore the tradeoffs between these quantities. The proposed formulation [(30) or (38)] provides an efficient method for evaluating these tradeoffs and, hence, should be a convenient tool for system designers.

The performance of the system in Example 4 can be significantly improved by using longer prototype filters or by reducing the downsampling factor K, although both actions will increase the implementation complexity of the system. Increasing the filter length to 200 results in SS-MSEs of around -27.1 dB for the interpolated symlet, and -28.6 dB and -29.7 dB for Harteneck's method and the proposed method, respectively, with the same distortion coefficient as the interpolated symlet; see [47] for the details. A reduction in the downsampling factor is considered in the following example.

Example 5: We consider the subband adaptive filtering system from Example 4 but with a downsampling factor of $K = 4$. The tradeoffs between the (normalized) stopband energy and distortion coefficient achieved by the three design methods are illustrated in Fig. 8. For the proposed method, we set the maximum spectral component constraint in the same way as in Example 1, and the maximum stopband level constraint was chosen to be that achieved by the interpolated symlet. (This constraint is inactive in the figure, as suggested by Table II.) The focus of this example is on the effects of the transition-band energy on the system performance. The solid, dotted, and dash-dot curves in Fig. 8 indicate the inherent tradeoffs (achieved by the proposed method) under different constraints on the transition-band energy. It is clear from Fig. 8 that (in this example) different constraints on the transition-band energy result in significantly different tradeoffs between the stopband energy and the distortion. In particular, Harteneck's method [19], which does not explicitly control the transition-band energy, achieves a tradeoff (indicated by the dashed curve) that is superior to that which can be achieved by any design method that imposes the transition-band energy constraints that we have chosen. (Recall that the proposed method achieves the *inherent* tradeoff for the given constraints, which is indicated by the dotted and dash-dot curves.) However, as illustrated in Table II and Fig. 9, filters designed via Harteneck's method may have rather large transition-band energies, and hence, improved state-state mean square error can be obtained using filters designed by the proposed method. (Since $K = 4$ in this example, we have used length 15 adaptive filters in the subbands in place of the length 10 adaptive filters in Example 4.) In particular, Table II indicates that for the same distortion coefficient as the interpolated symlet, the filter designed by Harteneck's method (symbol $\blacktriangledown$) performs only marginally better than the interpolated symlet (symbol $\times$). The filter designed by the proposed method without constraints on the transition-band energy (symbol $\bullet$) performs a little better (a gain of 0.7 dB in the SS-MSE). Constraining the transition-band energy of the filter to be less than or equal to that of the interpolated symlet improves performance by more than 1.3 dB (for a total gain over the interpolated symlet and Harteneck's method of around 2 dB, symbol $\blacksquare$), but overconstraining the transition-band energy results in a degradation in performance (symbol $\blacktriangle$).

If the required normalized distortion coefficient is reduced to 10^{-8}, the same trends apply, but the performance of filters designed by the proposed method improves, and their performance advantages increase. (The performance of Harteneck's filters actually degrades; symbol $\triangledown$.) In particular, the filter indicated by the symbol □ has a SS-MSE that is around 3.2 dB lower than that achieved by the interpolated symlet (symbol $\times$) and 3.3 dB lower than that achieved by the corresponding filter designed by Harteneck's method (symbol $\triangledown$). The convergence of the (averaged) output MSE of the subband adaptive filtering system for these and other representative filters is provided in Fig. 9. □

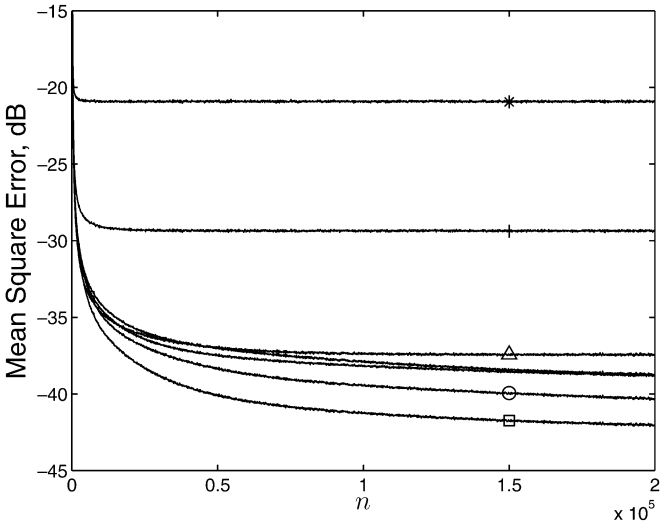

Fig. 9. Output mean square error (averaged over 1000 realizations) for Example 5. The symbols correspond to those in Table II and Fig. 8. The two curves without symbols correspond to Harteneck's method (marginally upper curve, symbol $\triangledown$) and the interpolated symlet (marginally lower curve, symbol $\times$).

TABLE II
PROTOTYPE FILTER CHARACTERISTICS AND STEADY-STATE MEAN SQUARE ERROR (SS-MSE) FOR THE ADAPTIVE FILTERING SYSTEM IN EXAMPLE 5

Design Method	Symbol in Fig. 8	γ_p^2/E_p,	rel. SBL, dB	$E_{P,\mathrm{sb}}/E_p$,	$E_{P,\mathrm{tb}}/E_p \times 10^{-2}$	SS-MSE, dB
Interp. [20], MSB [52],[53]	$*$	1.38×10^{-3}	-26.3	4.13×10^{-3}	8.86	-20.92
Interp. [20], Daubech. [51]	$+$	6.77×10^{-5}	-32.7	8.31×10^{-4}	7.14	-29.36
Interp. [20], symlet [51]	$\times$	1.42×10^{-5}	-43.6	3.62×10^{-5}	7.24	-38.83
Harteneck [19], $\lambda = 99.7$	$\blacktriangledown$	1.42×10^{-5}	-78.6	5.93×10^{-10}	8.86	-38.97
Proposed (38)	$\bullet$	1.42×10^{-5}	-85.7	1.27×10^{-10}	8.18	-39.58
Proposed (38)	$\blacksquare$	1.42×10^{-5}	-71.7	7.85×10^{-9}	7.24	-40.93
Proposed (38)	$\blacktriangle$	1.42×10^{-5}	-61.2	7.25×10^{-8}	5.79	-39.40
Harteneck [19], $\lambda = 0.642$	$\triangledown$	10^{-8}	-66.5	9.19×10^{-9}	10.0	-38.76
Proposed (38)	$\circ$	10^{-8}	-83.2	3.12×10^{-10}	8.81	-40.35
Proposed (38)	$\square$	10^{-8}	-60.1	9.52×10^{-8}	7.24	-42.05
Proposed (38)	$\triangle$	10^{-8}	-58.2	1.18×10^{-6}	5.79	-37.44

VII. CONCLUSIONS

In this paper, we have derived explicit bounds on the aliasing in the subbands and the output, the distortion, and the imaged subband errors of an oversampled near perfect reconstruction (and near paraunitary) GDFT filterbank. We have shown that the design of a prototype filter that optimizes these bounds can be formulated as a convex optimization problem from which a globally optimal filter can be efficiently obtained. The key to developing the convex formulation was to show that the performance objectives can be written as linear and convex quadratic functions of the autocorrelation sequence of the filter. We showed that the convex formulation allows efficient and accurate exploration of the inherent tradeoffs in the design and generates filters with significantly improved performance over two current techniques. Since the intersection of convex sets is itself convex, the proposed method is quite flexible, and several other performance objectives can be incorporated into the design [47], [56]; see also [30], [31], [34], and [48]. Furthermore, it appears that variations on the proposed method may also be applicable to the design of windows for oversampled short-term Fourier transforms that form a "snug" frame [57] and the design of filtered multitone modulation schemes [58].

APPENDIX
DERIVATION OF (28)

Given (23)

$$E_D \le E_x \max_{\omega} \left| \frac{1}{K} \sum_{m=0}^{M-1} \left| P(e^{j(\omega-\alpha_m)}) \right|^2 - 1 \right|^2. \qquad (42)$$

Now

$$\begin{aligned} &\frac{1}{K} \sum_{m=0}^{M-1} \left| P(e^{j(\omega-\alpha_m)}) \right|^2 \\ &\quad = \frac{1}{K} \sum_{k,\ell} p[k]p[\ell] e^{-j(\omega - m_0/M)(k-\ell)} \sum_{m=0}^{M-1} e^{j2\pi m(k-\ell)/M} \\ &\quad = \frac{M}{K} \sum_{n} \left(\sum_{\ell} p[\ell]p[\ell+Mn] \right) e^{-j(\omega M - 2\pi m_0)n} \qquad (43) \end{aligned}$$

where we have used the Poisson sum formula. Hence

$$\begin{aligned} &\max_{\omega} \left| \frac{1}{K} \sum_{m=0}^{M-1} \left| P(e^{j(\omega-\alpha_m)}) \right|^2 - 1 \right|^2 \\ &\quad \le \frac{M}{K} \left| \sum_{n} \left(\sum_{\ell} p[\ell]p[\ell+Mn] \right) - \delta[n] \right|^2 \\ &\quad \le \frac{M}{K} \left(\sum_{n} \left| \left(\sum_{\ell} p[\ell]p[\ell+Mn] \right) - \delta[n] \right| \right)^2. \qquad (44) \end{aligned}$$

Equation (28) then follows from the normalization of the prototype filter $\sum_\ell p[\ell]^2 = K/M$ and the definition of $\tilde{\gamma}_p$.

REFERENCES

[1] R. E. Crochiere and L. R. Rabiner, *Multirate Digital Signal Processing*. Englewood Cliffs, NJ: Prentice-Hall, 1983.

[2] P. Vaidyanathan, *Multirate Systems and Filterbanks*. Englewood Cliffs, NJ: Prentice-Hall, 1993.

[3] M. Vetterli and J. Kovačević, *Wavelets and Subband Coding*. Englewood Cliffs, NJ: Prentice-Hall, 1995.

[4] G. Strang and T. Nguyen, *Wavelets and Filterbanks*. Wellesley, MA: Wellesley-Cambridge, 1997.

[5] Z. Cvetković and M. Vetterli, "Oversampled filterbanks," *IEEE Trans. Signal Processing*, vol. 46, pp. 1245–1255, May 1998.

[6] H. Bölcskei, F. Hlawatsch, and H. G. Feichtinger, "Frame-theoretic analysis of oversampled filterbanks," *IEEE Trans. Signal Processing*, vol. 46, pp. 3256–3268, Dec. 1998.

[7] P. N. Heller, T. Karp, and T. Q. Nguyen, "A general formulation of modulated filterbanks," *IEEE Trans. Signal Processing*, vol. 47, pp. 986–1002, Apr. 1999.

[8] Z. Cvetković and M. Vetterli, "Tight Weyl-Heisenberg frames in $\ell^2(\mathbb{Z})$," *IEEE Trans. Signal Processing*, vol. 46, pp. 1256–1259, May 1998.

[9] J. Kliewer and A. Mertins, "Oversampled cosine-modulated filterbanks with arbitrary system delay," *IEEE Trans. Signal Processing*, vol. 46, pp. 941–955, Apr. 1998.

[10] H. Bölcskei and F. Hlawatsch, "Oversampled cosine modulated filterbanks with perfect reconstruction," *IEEE Trans. Circuits Syst. II*, vol. 45, pp. 1057–1071, Aug. 1998.

[11] M. K. Mıhçak, P. Moulin, M. Anitescu, and K. Ramchandran, "Rate-distortion-optimal subband coding without perfect reconstruction constraints," *IEEE Trans. Signal Processing*, vol. 49, pp. 542–557, Mar. 2001.

[12] J. J. Shynk, "Frequency-domain and multirate adaptive filtering," *IEEE Signal Processing Mag.*, vol. 9, pp. 15–37, Jan. 1992.

[13] A. Gilloire and M. Vetterli, "Adaptive filtering in subbands: Analysis, experiments, and application to acoustic echo cancellation," *IEEE Trans. Signal Processing*, vol. 40, pp. 1862–1875, Aug. 1992.
[14] Q. Jin, Z. Q. Luo, and K. M. Wong, "Optimum filterbanks for signal decomposition and its application in adaptive echo cancelation," *IEEE Trans. Signal Processing*, vol. 44, pp. 1669–1680, July 1996.
[15] B. Farhang-Boroujeny and Z. Wang, "Adaptive filtering in subbands: Design issues and experimental results for acoustic echo cancellation," *Signal Process.*, vol. 61, pp. 213–223, 1997.
[16] S. Weiss, A. Stenger, R. W. Stewart, and R. Rabenstein, "Steady-state performance limitations of subband adaptive filters," *IEEE Trans. Signal Processing*, vol. 49, pp. 1982–1991, Sept. 2001.
[17] J. P. Reilly, M. Wilbur, M. Seibert, and N. Ahmadvand, "The complex subband decomposition and its application to the decimation of large adaptive filtering problems," *IEEE Trans. Signal Processing*, vol. 50, pp. 2730–2743, Nov. 2002.
[18] M. Harteneck, J. M. P. Borrallo, and R. W. Stewart, "An oversampled subband adaptive filter without cross adaptive filters," *Signal Process.*, vol. 64, no. 1, pp. 93–101, 1998.
[19] M. Harteneck, S. Weiss, and R. W. Stewart, "Design of near perfect reconstruction oversampled filterbanks for subband adaptive filters," *IEEE Trans. Circuits Syst. II*, vol. 46, pp. 1081–1085, Aug. 1999.
[20] Q.-G. Liu, B. Champagne, and D. K. C. Ho, "Simple design of oversampled uniform DFT filterbanks with applications to subband acoustic echo cancellation," *Signal Process.*, vol. 80, no. 5, pp. 831–847, 2000.
[21] K. Eneman and M. Moonen, "Hybrid subband/frequency-domain adaptive systems," *Signal Process.*, vol. 81, pp. 117–136, 2001.
[22] ——, "DFT modulated filterbank design for oversampled subband systems," *Signal Process.*, vol. 81, pp. 1947–1973, 2001.
[23] M. R. Petraglia and S. K. Mitra, "Performance analysis of adaptive filter structures based on subband decomposition," in *Proc. Int. Symp. Circuits Syst.*, vol. I, Chicago, IL, 1993, pp. 60–63.
[24] *Handbook of Global Optimization*, R. Horst and P. M. Pardalos, Eds., Kluwer, Dordrecht, The Netherlands, 1995.
[25] M. Vetterli, "Filterbanks allowing perfect reconstruction," *Signal Process.*, vol. 10, pp. 219–244, 1986.
[26] T. Q. Nguyen, "Digital filterbank design: Quadratic-constrained formulation," *IEEE Trans. Signal Processing*, vol. 43, pp. 2103–2105, Sept. 1995.
[27] H. Xu, W.-S. Lu, and A. Antoniou, "Efficient iterative design method for cosine-modulated QMF banks," *IEEE Trans. Signal Processing*, vol. 44, pp. 1657–1668, July 1996.
[28] M. C. Jeruchim, P. Balaban, and K. S. Shanmugan, *Simulation of Communication Systems*, Second ed. New York: Kluwer, 2000.
[29] R. D. Koilpillai and P. P. Vaidyanathan, "Cosine-modulated FIR filterbanks satisfying perfect reconstruction," *IEEE Trans. Signal Processing*, vol. 40, pp. 770–783, Apr. 1992.
[30] S.-P. Wu, S. Boyd, and L. Vandenberghe, "FIR filter design via spectral factorization and convex optimization," in *Applied Computational Control, Signal and Communications*, B. Datta, Ed. Boston, MA: Birkhäuser, 1997.
[31] T. N. Davidson, Z.-Q. Luo, and J. F. Sturm, "Linear matrix inequality formulation of spectral mask constraints with applications to FIR filter design," *IEEE Trans. Signal Processing*, vol. 50, pp. 2702–2715, Nov. 2002.
[32] P. Moulin, M. Anitescu, K. O. Kortanek, and F. A. Potra, "The role of linear semi-infinite programming in signal adapted QMF bank design," *IEEE Trans. Signal Processing*, vol. 45, pp. 2160–2174, Sept. 1997.
[33] J. Tuqan and P. P. Vaidyanathan, "A state space approach to the design of globally optimal FIR energy compaction filters," *IEEE Trans. Signal Processing*, vol. 48, pp. 2822–2838, Oct. 2000.
[34] T. N. Davidson, "Efficient design of waveforms for robust pulse amplitude modulation," *IEEE Trans. Signal Processing*, vol. 49, pp. 3098–3111, Dec. 2001.
[35] T. N. T. Goodman, C. A. Micchelli, G. Rodriguez, and S. Seatzu, "Spectral factorization of Laurent polynomials," *Adv. Comput. Math.*, vol. 7, no. 4, pp. 429–454, 1997.
[36] R. D. Koilpillai and P. P. Vaidyanathan, "A spectral factorization approach to psuedo-QMF design," *IEEE Trans. Signal Processing*, vol. 41, pp. 82–92, Jan. 1993.
[37] W. A. Gardner, *Statistical Spectral Analysis. A Non-probabilistic Theory*. Englewood Cliffs, NJ: Prentice-Hall, 1988.
[38] W. Rudin, *Real and Complex Analysis*. New York: McGraw-Hill, 1987.
[39] J. W. Adams and J. L. Sullivan, "Peak-constrained least-squares optimization," *IEEE Trans. Signal Processing*, vol. 46, pp. 306–321, Feb. 1998.
[40] R. Hettich and K. O. Kortanek, "Semi-infinite programming: Theory, methods and applications," *SIAM Rev.*, vol. 35, no. 3, pp. 380–429, 1993.
[41] M. Lobo, L. Vandenberghe, S. Boyd, and H. Lebret, "Applications of second-order cone programming," *Linear Algebra Applications*, vol. 284, pp. 193–228, 1998.
[42] A. Papoulis, *Signal Analysis*. New York: McGraw-Hill, 1977.
[43] L. Vandenberghe and S. Boyd, "Semidefinite programming," *SIAM Rev.*, vol. 38, 1996.
[44] J. F. Sturm, "Using SeDuMi 1.02, a Matlab toolbox for optimization over symmetric cones," *Optimiz. Methods Softw.*, vol. 11–12, pp. 625–653, 1999.
[45] B. Alkire and L. Vandenberghe, "Interior-point methods for magnitude filter design," in *Proc. Int. Conf. Acoust., Speech, Signal Processing*, Salt Lake, UT, May 2001, pp. 3821–3824.
[46] M. R. Wilbur, T. N. Davidson, and J. P. Reilly, "Efficient design of oversampled NPR GDFT filterbanks," in *Proc. Int. Conf. Acoust., Speech, Signal Process.*, vol. VI, Hong Kong, Apr. 2003, pp. 489–492.
[47] ——, (2003) Efficient Design of Oversampled NPR GDFT Filterbanks, Manuscript. Dept. Elect. Comput. Eng., McMaster Univ., Hamilton, ON, Canada. [Online]. Available: http://www.ece.mcmaster.ca/~davidson
[48] T. N. Davidson, Z.-Q. Luo, and K. M. Wong, "Design of orthogonal pulse shapes for communications via semidefinite programming," *IEEE Trans. Signal Processing*, vol. 48, pp. 1433–1445, May 2000.
[49] Y. Neuvo, C. Y. Dong, and S. K. Mitra, "Interpolated finite impulse response filters," *IEEE Trans. Acoust., Speech, Signal Processing*, vol. ASSP-32, pp. 563–570, Dec. 1984.
[50] R. Lyons, "Interpolated narrowband lowpass FIR filters," *IEEE Signal Processing Mag.*, vol. 20, pp. 50–57, Jan. 2003.
[51] I. Daubechies, *Ten Lectures on Wavelets*. Philadelphia, PA: SIAM, 1992.
[52] F. Mintzer, "Filters for distortion-free two-band multirate filterbanks," *IEEE Trans. Acoust., Speech, Signal Processing*, vol. ASSP-33, pp. 626–630, June 1985.
[53] M. J. T. Smith and T. P. Barnwell III, "Exact reconstruction techniques for tree-structured subband coders," *IEEE Trans. Acoust., Speech, Signal Processing*, vol. ASSP-34, pp. 434–441, June 1986.
[54] F. J. Harris, "On the use of windows for harmonic analysis with the discrete Fourier transform," *Proc. IEEE*, vol. 66, pp. 51–83, Jan. 1978.
[55] S. Haykin, *Adaptive Filter Theory*, Fourth ed. Upper Saddle River, NJ: Prentice-Hall, 2002.
[56] M. R. Wilbur, "The decomposition of large blind equalization problems using GDFT filterbanks," Master's thesis, McMaster Univ., Hamilton, ON, Canada, 2000.
[57] Z. Cvetković, "On discrete short-time Fourier analysis," *IEEE Trans. Signal Processing*, vol. 48, pp. 2628–2640, Sept. 2000.
[58] G. Cherubini, E. Eleftheriou, and S.Ölçer, "Filtered multitone modulation for very high-speed digital subscriber lines," *IEEE J. Select. Areas Commun.*, vol. 20, pp. 1016–1028, June 2002.

Matthew R. Wilbur (M'94) was born in Ontario, Canada. He received the B.Eng.S. and M.Eng. degrees from McMaster University, Hamilton, ON, in 1998 and 2000, respectively. His thesis research investigated the use of subbanding for the decimation of large problems and the convex design of prototype filters for filterbanks.

He has worked as a radio frequency intgrated circuit design engineer for Sirenza Microdevices, Ottawa, ON, on high-performance RF signal processing circuits for wireless basestation transceiver systems.

Mr. Wilbur received an NSERC post-graduate scholarship and the prestigious Fessenden Postgraduate Scholarship from CRC/Industry Canada.

Timothy N. Davidson (M'96) received the B.Eng. (Hons. I) degree in electronic engineering from The University of Western Australia (UWA), Perth, Australia, in 1991 and the D.Phil. degree in engineering science from the The University of Oxford, Oxford, U.K., in 1995.

He is currently an assistant professor with the Department of Electrical and Computer Engineering, McMaster University, Hamilton, ON, Canada. His research interests are in signal processing, communications, and control, with current activity focused on signal processing for digital communication systems. He has held research positions at the Communications Research Laboratory at McMaster University, the Adaptive Signal Processing Laboratory at UWA, and the Australian Telecommunications Research Institute, Curtin University of Technology, Perth.

Dr. Davidson received the 1991 J. A. Wood Memorial Prize (for "the most outstanding [UWA] graduand" in the pure and applied sciences) and the 1991 Rhodes Scholarship for Western Australia.

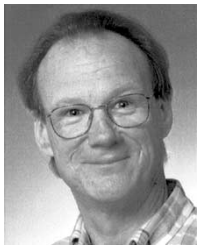

James P. Reilly (S'76–M'80) received the B.A.Sc. degree from the University of Waterloo, Waterloo, ON, Canada, in electrical engineering in 1973 and the M.Eng. and Ph.D. degrees from McMaster University, Hamilton, ON, in 1977 and 1980, respectively, both in electrical engineering.

From 1973 to 1975, he was with the CATV industry, designing RF distribution equipment, and from 1980 to 1985, he was with Bell-Northern Research, Ottawa, ON, where he was involved in the development of terrestrial microwave radio for digital transmission systems. He joined the faculty at McMaster University in 1985 as an associate professor and was promoted to the rank of full professor in 1992. His research interests are in several aspects of signal processing, specifically blind signal separation, blind signal identification, array signal processing, and Bayesian methods.

Prof. Reilly is a registered professional engineer in the province of Ontario.